# Progress Report on Alloy 617 Time-Dependent Allowable Stresses
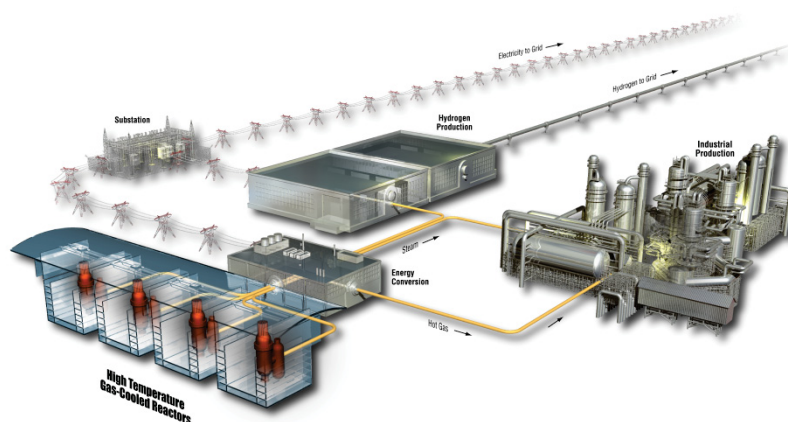
Jill K. Wright
Thomas M. Lillo

June 2015

INL
Idaho National Laboratory

# Progress Report on
# Alloy 617 Time-Dependent Allowable Stresses

**Jill K. Wright**
**Thomas M. Lillo**

**June 2015**

**Idaho National Laboratory**
**INL ART Program**
**Idaho Falls, Idaho 83415**

**http://www.inl.gov**

**INL ART Program**

# Progress Report on
# Alloy 617 Time-Dependent Allowable Stresses

**INL/EXT-15-35640**
**Revision 0**

**June 2015**

**Author:**
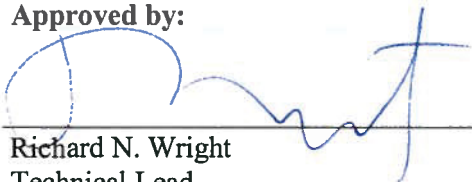
_____     6/29/15
Jill K. Wright                                      Date
Staff Scientist


**Approved by:**

_____     6/29/2015
Richard N. Wright                                 Date
Technical Lead

_____     6/30/2015
Travis R. Mitchell                                Date
INL ART TDO Relationship Manager

_____     6/30/2015
Kirk W. Bailey                                    Date
INL ART TDO Quality Assurance

# ABSTRACT

Time-dependent allowable stresses are required in the American Society of Mechanical Engineers (ASME) Boiler and Pressure Vessel Code for design of components in the temperature range where time-dependent deformation (i.e., creep) is expected to become significant. There are time-dependent allowable stresses in ASME, Section II Part D, for use in the non-nuclear construction codes. However, additional criteria must be considered to develop time-dependent allowable stresses for nuclear components, which are specified in ASME, Section III, Division 1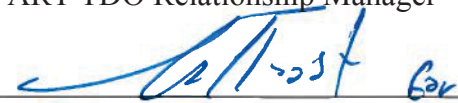 — Subsection NH. The time-dependent Allowable Stress Intensity Value, $S_t$, is defined as the lesser value of 100% of the average stress required to obtain a total (elastic, plastic, and primary and secondary creep) strain of 1%, 67% of the minimum stress to cause rupture, and 80% of the minimum stress to cause initiation of tertiary creep. $S_t$ values are reported for a range of temperatures and time increments up to 100,000 hours. These values are determined from uniaxial creep tests, which involve the elevated-temperature application of a constant load that is relatively small, resulting in deformation over a long time period prior to rupture. $S_r$, minimum stress-to-rupture values, are also required for Section III, Subsection NH materials and are reported here as well.

In this report data from a large number of creep and creep-rupture tests on Alloy 617 were analyzed using the ASME Section III NH criteria. Data that were used in the analysis are from the ongoing Department of Energy-sponsored High Temperature Materials Program, the Korean Atomic Energy Research Institute through the Generation IV Very High Temperature Reactor Materials Program, and historical data from previous high-temperature-reactor research and vendor data generated in developing the alloy.

It is found that the tertiary creep criterion determines the $S_t$ value at highest temperatures, while the stress to cause 1% total strain controls at low temperatures. The ASME Section III Working Group on Allowable Stress Criteria recommended that the uncertainties associated with determining the onset of tertiary creep and the lack of significant cavitation associated with early tertiary creep strain suggest that the tertiary creep criterion is not appropriate for Alloy 617. If the tertiary creep criterion is dropped from consideration, the stress to rupture criterion determines the $S_t$ value at all but the lowest temperatures.

# CONTENTS

# FIGURES

# TABLES

# ACRONYMS

ANL      Argonne National Laboratory

ART      Advanced Reactor Technologies

ASME      American Society of Mechanical Engineers

B&PV      Boiler and Pressure Vessel

GIF      Generation IV International Forum

INL      Idaho National Laboratory

KAERI      Korean Atomic Energy Research Institute

SMC      Special Metals Corporation

TEM      Transmission Electron Microscopy

VHTR      Very High Temperature Gas-Cooled Reactor

# Progress Report on
# Alloy 617 Time-Dependent Allowable Stresses

## 1.    INTRODUCTION

Alloy 617 is the primary candidate material for the heat exchanger of a very high temperature gas-cooled reactor (VHTR) intended to operate up to 950°C. While this alloy is currently qualified in the American Society of Mechanical Engineers (ASME) Boiler and Pressure Vessel (B&PV) Code for non-nuclear construction, it is not currently allowed for use in nuclear designs. Extensive characterization of Alloy 617 properties began in the 1970s and accelerated greatly with the high temperature gas-cooled reactor programs that were carried out internationally through the early 1990s. A draft ASME Code Case to qualify Alloy 617 for nuclear pressure boundary applications was submitted in 1992, but was withdrawn prior to approval. Recently, the interest in VHTR technology for process heat applications has resulted in a renewed interest in Alloy 617, which has superior resistance to creep at temperatures greater than about 650°C compared to iron-based austenitic alloys.

One of the critical values required by the ASME B&PV Code for use in elevated temperature nuclear design (Section III, Subsection NH[1][a]) is the time-dependent Allowable Stress Intensity Value, $S_t$ (also known as the time-dependent allowable stress). These values are determined from uniaxial creep tests, which involve the elevated temperature application of a constant load that is relatively small, resulting in deformation over a long time period prior to rupture. $S_t$ is defined as the lesser of three quantities: 100% of the average stress required to obtain a total (elastic, plastic, primary and secondary creep) strain of 1%, 67% of the minimum stress to cause rupture, and 80% of the minimum stress to cause the initiation of tertiary creep. The values are reported for a range of temperatures from 800°F (427°C) to the maximum use temperature of the alloy, and for logarithmic time increments up to 100,000 hours.  Time-dependent stress values also must be considered at elevated temperatures when determining the Maximum Allowable Stress Values, $S$, in ASME Section II, Part D [2]; however, a different set of criteria are used to determine the $S$ values, all based on behavior at 100,000 hours. Section II values are not the subject of this report.

The strain to 1% and rupture criteria are used to limit the overall deformation of a component and actual failure, respectively. ASME adopted the tertiary creep criterion after it was observed experimentally that internally-pressurized tubes of austenitic stainless steel leaked due to creep damage at times less than those predicted using analysis based on uniaxial rupture data. In the absence of extensive experimental tube failure data over a range of relevant temperatures, this criterion was developed based on the logic that the onset of tertiary creep during uniaxial testing of austenitic stainless steels is associated with extensive creep induced cavitation. Eliminating tertiary creep, and the associated cavitation, was presumed to represent a conservative indirect limit to minimize the potential for premature failure of tubes under multi-axial loading.

Many engineering materials exhibit a classical creep response with three distinct regimes – primary creep, secondary creep, and tertiary creep – in which most of the creep behavior occurs during the linear secondary creep regime, prior to the relatively brief period of accelerated creep of the tertiary regime. For many temperatures and stresses of interest for VHTR applications, Alloy 617 exhibits only brief secondary creep or an inflection between the primary creep regime and extensive tertiary creep prior to rupture, rather than a distinct linear secondary creep regime. This has raised questions regarding the validity of the tertiary creep criterion for the $S_t$ value for Alloy 617 as well as some other alloys that exhibit similar creep behavior.

---

[a] Subsection NH will be incorporated in Section III, Div. 5, Subsection HBB effective with the 2015 edition of the ASME B&PV Code to be released in July 2015. Since this new issue is not generally available as of the release of this report, the references to Subsection NH will be maintained herein.

Preliminary $S_t$ values are reported here for Alloy 617. The origin of the creep data used in the analysis is reviewed, and the procedure for determining $S_t$ is explained. The validity of the tertiary creep criterion is discussed and the effect of eliminating the tertiary creep criterion on the value of $S_t$ has been examined. The minimum stress to rupture, $S_r$, which is also required for the Alloy 617 Code Case and is calculated in the process of determining creep-rupture criterion for $S_t$. These values are presented as well.

## 2. SOURCES OF CREEP DATA

When calculating allowable stress values for an alloy, it is desirable to use properties of as many different heats and product forms as possible. To accomplish this for Alloy 617, data have been assembled from three general sources; testing of modern heats of Alloy 617 plate in current VHTR programs, historical data from previous high-temperature reactor programs, and data originally generated by the vendor developing Alloy 617. The data set has been limited to specimens that were tested in air.

## 2.1 Idaho National Laboratory Creep Testing

The United States Advanced Reactor Technologies (ART) Program (previously VHTR) maintains a creep testing program of Alloy 617 that has been ongoing for a number of years. The creep testing program for Alloy 617 includes tests interrupted at a predetermined strain level, as well as tests run until specimen rupture occurred. Several additional stress rupture tests are in-progress with expected durations of up to 7 years.

The majority of the work in this creep testing program was done at Idaho National Laboratory (INL) using cylindrical creep specimens with a nominal 6.35-mm reduced section diameter and a gage length of 34.2 mm, that were machined from an Alloy 617 solution-annealed plate in conformance with ASTM-E139-06.[3] Additional testing, reported below, was also carried out on this plate material at Argonne National Laboratory (ANL). The specimens were machined with their longitudinal axis oriented along the rolling direction of a 37-mm-thick plate provided by ThyssenKrupp VDM (composition given in Table 1). Although inhomogeneity exists in the microstructure, the average grain size measured by the linear intercept method is 150 μm.

Table 1. Chemical composition of the Alloy 617 Plate tested at INL and ANL.

| Chemical Composition (wt%) | | | | | | | | | | | | |
|------|------|------|------|------|------|------|------|------|------|------|--------|--------|
| Ni | Cr | Co | Mo | Al | Ti | Fe | Mn | Cu | Si | C | S | B |
| Bal. | 22.2 | 11.6 | 8.6 | 1.1 | 0.4 | 1.6 | 0.1 | 0.04 | 0.1 | 0.05 | <0.002 | <0.001 |

High-temperature creep tests were conducted at multiple stresses at 750, 800, 900, and 1000°C using Applied Test Systems (Applied Test Systems, Inc., Butler, PA) lever arm creep frames with dead weight loading. The temperature of the gage section of the creep specimen was measured with Type-K thermocouples for tests at temperatures of 800°C and less and Type-R thermocouples for tests at temperatures of 900°C and greater. The specimen temperature was controlled throughout the test to within ±3 K of the target test temperature. Dual-averaging linear variable differential transformer (LVDT) transducers or Heidenheim linear encoded photoelectric gages were used to monitor creep strain during the creep tests to a resolution of better than 0.01% strain. Tests were interrupted when the creep strain had attained a predetermined target value for microstructure characterization or terminated when the specimen ruptured. The final creep strain was determined by measuring the increase in sample length after cooling to room temperature and removing from the creep frame.

In order to elucidate the mechanism responsible for tertiary creep in Alloy 617, extensive microstructural characterization was carried out on creep specimens where the test was terminated prior to failure. Interrupted creep tests were run to a total creep strain of approximately 2, 5, 10, and 20%, primarily at 750 or 1000°C, and cooled under load to preserve the deformed microstructure for metallurgical evaluation. Additional creep tests were run to a creep strain of 20% at 1000°C under various creep stresses to provide additional insight into the effect of initial creep stress on creep behavior and creep void fraction. A few creep tests were run to a total creep strain of 20% at 800 and 900°C to gain a better understanding of the effect of temperature on the resulting creep void area fraction.

The gage section (including the minimum gage diameter) of each specimen from each interrupted test was prepared for optical metallography and mounted to produce a longitudinal section along the gage length. After mechanical polishing down to 3- micron alumina, the entire polished gage section was electropolished (Struers LectroPol-5) in a solution of ethanol-10% water-10% ethylene glycol monobutyl ether-7% perchloric acid to remove flowed metal from the creep voids that may have occurred during mechanical polishing. Metallography samples were then subjected to vibratory polishing using 0.05- micron colloidal silica for 1 hour. Automated image acquisition (Zeiss Axio Observer.Z1M) of the entire gage section was carried out at 200x. The area of each individual photograph was approximately 0.4 mm$^2$ while the total area of the gage section analyzed was on the order of 80 mm$^2$ (approximately 200 photographs covering the gage length). Following this initial porosity analysis, approximately 200-500 μm of material were removed from the metallography mounts and the porosity analysis was repeated to ensure that the porosity was homogeneously distributed throughout the gage section. The porosity analysis was repeated a third time after removing an additional 200-500 μm of material. Approximately 240 mm$^2$ of area was analyzed through the gage section of each sample. Each photograph from the three sections was individually analyzed for porosity using image analysis (AxioVision 4, version 4.8.2.0) and reported as a percentage of the image area.

Part of the reduced gage section was reserved for making transmission electron microscopy (TEM) samples to look for creep cavitation at length scales below the resolution of optical metallography and to characterize the dislocation structure. TEM samples were made with orientations parallel (longitudinal) and perpendicular (transverse) to the stress axis of the creep sample. At least 10 samples from the gage section of selected interrupted creep samples were examined using TEM.

## 2.2    Generation IV International Forum Database

The Generation IV International Forum (GIF) VHTR Materials Program Management Board has agreed to compile data from earlier testing programs and share data generated from current member test programs in the GIF Materials Handbook.[4] Past creep data include those generated at Huntington Alloys (the original producer of Inconel 617 and now part of Special Metals Corporation (SMC)), as well as General Electric and Oak Ridge National Laboratory as part of the Department of Energy High-Temperature Gas-Cooled Reactor Research Program of the 1980s and 1990s. Creep curves (i.e., strain vs. time) are not available for all of these creep tests, and the inclusion of other details (e.g., creep rate, time to 1% creep strain) varies among and within the laboratories. Some details of the testing procedure are also unknown. Data from these three laboratories represent 16 heats of the alloy and multiple product forms, including plate, sheet, and rod.

More recently, creep data have been contributed by INL, ANL [5], and the Korean Atomic Energy Research Institute (KAERI).[6,7,8,9] Somewhat more is known regarding creep test procedures of these organizations. Data represent three heats of material, all in plate form.

### 2.2.1    Argonne National Laboratory Creep Testing

Creep testing at ANL was conducted as part of a study of the creep properties of weldments [5], which included standard creep specimens machined from plate as well as the cross-welded specimens. Specimens were machined from the same plate described in Subsection 2.1 and had a nominal reduced

section diameter of 4 mm and length of 19 mm. Testing was conducted at 750, 850, and 950°C. Creep testing was carried out in conformance with ASTM-E-139-11.[10] Prior to testing, the creep specimen was loaded into the split-collet grips and pull rod assembly supported by a setup jig. Calibrated Type-K thermocouples were spot welded to the specimen outer transition radius shoulder edge so as not to introduce defects into the gage length area. Direct-load Applied Test Systems creep frames were used to test specimens at 850 and 950°C. A three-zone furnace was used to heat to the test temperature setpoint over a 3-hour ramp time. The test specimen was centered in the middle furnace zone and the specimen temperature profile maintained within ±1ºC of the desired test temperature.

## 2.2.2    Korean Atomic Energy Research Institute Creep Testing

Specimens for creep testing at KAERI were machined from commercial-grade Alloy 617 solution annealed hot-rolled plate produced by SMC, with a thickness of 16 mm. The chemical composition is shown in Table 2. The grain size was approximately 300 µm. Cylindrical creep specimens had a 30 mm gauge length and a 6 mm diameter, with the axis aligned with the rolling direction. Creep tests were conducted at temperatures of 850, 900, and 950°C, controlled to ±2°C during testing. A range of stress levels was tested; however, stress levels of 30 and 35 MPa were tested for each temperature. Strain was measured using an extensometer and creep rates were obtained from the creep curves.[6,7,9]

Additional tests were conducted at 800°C on specimens of the same geometry from an approximately 16-mm thick plate of a different composition [8], also shown in Table 2. Stress levels of 60-100 MPa were tested in air, using Type-K thermocouples to monitor the temperature within the split three-zone furnace used for heating the specimen.

Table 2. Chemical composition of alloy 617 plate tested at KAERI.

| Parameter | Chemical Composition (wt%) | | | | | | | | | | | | |
| | Ni | Cr | Co | Mo | Al | Ti | Fe | Mn | Cu | Si | C | S | B |
|---|---|---|---|---|---|---|---|---|---|---|---|---|---|
| KAERI | Bal. | 22.16 | 11.58 | 9.8 | 1.12 | 0.35 | 1.5 | 0.1 | 0.08 | 0.06 | 0.08 | 0.001 | 0.002 |
| KAERI (800°C) | Bal. | 22.2 | 12.3 | 9.5 | 1.06 | 0.41 | 0.949 | 0.029 | 0.027 | 0.084 | 0.08 | <0.002 | <0.002 |

# 2.3    Creep data from the Literature

Additional creep data have been published in scientific literature. Discussion with members of the ASME Section III Working Group on Allowable Stress Criteria suggested that a subset of these data could be incorporated into the data set used to determine allowable stresses for Alloy 617 provided there was known chemistry for the material. Two sources met this criterion, as discussed in Subsections 2.3.1 and 2.3.2.

## 2.3.1    Cook

Cook [11] reports data from creep tests conducted in air at temperatures from 800 to 950°C at 50°C increments, primarily machined from a 25-mm bar, but including a few specimens from a 12-mm bar and one from a 12-mm plate, representing three different heats. The grain sizes are reported as ASTM grain numbers of 4, 2.5, and 1.5, respectively. Data were reported in graphical form and required digitization to obtain rupture time and stress. Specimens were nominally 4.53 mm in diameter and strain was determined by measuring the distance between gage marks approximately every 1000 hours.

## 2.3.2    Chomette

Chomette [12] reports data from five specimens, 5 mm in diameter, machined from a single heat of 50-mm-diameter hot rolled bar stock with a grain size of 270 µm and tested in air at 850 or 950°C. Stress, temperature, and rupture time are tabulated for each test.

# 3. LARSON-MILLER PLOTS

The most common method for comparing creep-rupture tests performed at various temperatures and stress levels is by plotting stress against the Larson-Miller parameter (LMP):

$$LMP = T (C + \log t_R) \tag{1}$$

*where* T is absolute temperature, C is the Larson-Miller constant and $t_R$ is time to rupture.[13] A stress function is formulated using a second-order polynomial in log stress:

$$LMP = a_0 + a_1 \log S + a_2 (\log S)^2 \tag{2}$$

For the purposes of the regression analysis, the stress function is rewritten so that $\log t_R$ is the dependent variable and T and log S are the independent variables:

$$\log t_R = \left[ \frac{a_0 + a_1 \log S + a_2 (\log S)^2}{T} \right] - C \tag{3}$$

Using a least squares fitting method, the optimum values for C, $a_0$, $a_1$ and $a_2$ are determined. A "lot-centering" procedure developed by Sjodahl [14] was employed that calculates the lot constant ($C_{lot}$) for each heat of material, along with the Larson-Miller constant, C, which is the average of the lot constants. A spreadsheet developed for ASME (referred to as the Swindeman spreadsheet after its authors) [15] was used to generate the Larson-Miller plots used in this report.

## 3.1  Stress-Rupture

A Larson-Miller plot (Figure 1) was created using a data set comprised of information from 296 creep specimens with known chemistry. Regression analysis for a second-order polynomial fit produced a correlation coefficient $R^2 = 0.9961$, C = 17.39 in Equation (1) and $a_0 = 33,381$ $a_1 = -5304.3$ and $a_2 = -217.36$ in Equation (2).
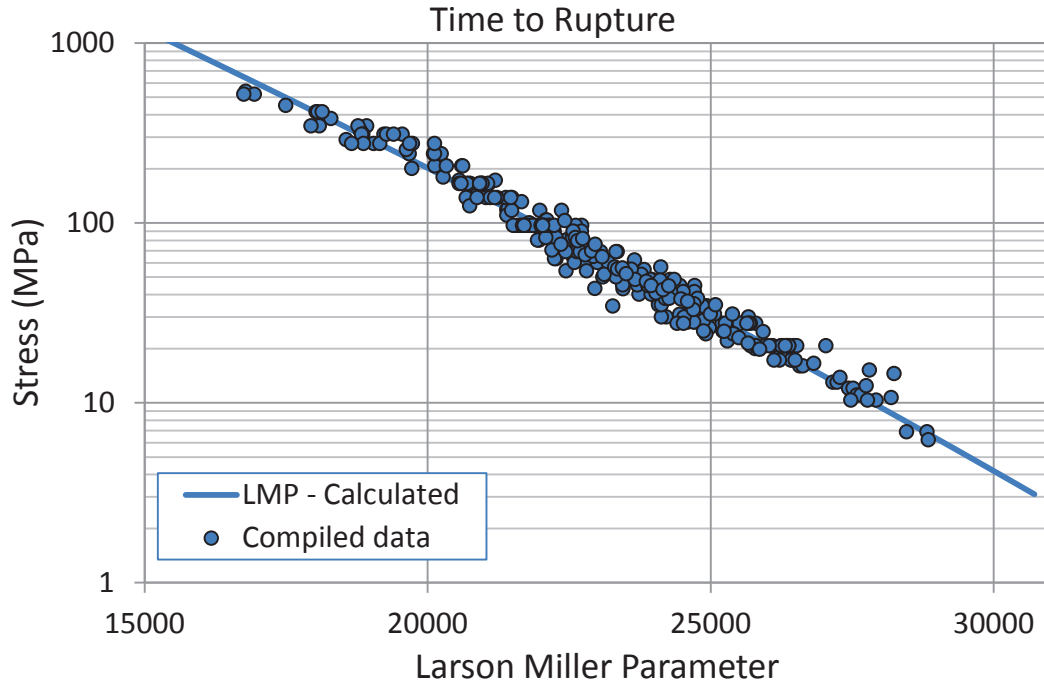


Figure 1. Larson-Miller plot with second-order polynomial fit for time to creep rupture of Alloy 617.

Results from the majority of the INL, ANL, and KAERI studies fall in the lower portion of the complete data set. There are two possible sources of this apparent difference in rupture behavior. It is now standard practice for all of the vendors of contemporary heats of Alloy 617 to use the additional step of electro-slag remelting prior to casting ingots; this was not typical for the historical heats. There is also a systematic trend for modern heats of Alloy 617 to have cobalt content below 12% (typically replaced by increasing iron) while the majority of historical data were measured from heats with Co content above 12%. There are a few data for a modern heat of Alloy 617 from the KAERI testing program that has Co content above 12%. Plotting these data on the Larson-Miller plot shows that they fit with the trend of historical values, suggesting that it is the alloy chemistry and not the melt practice that results in lower rupture life in the modern material, as shown in Figure 2.
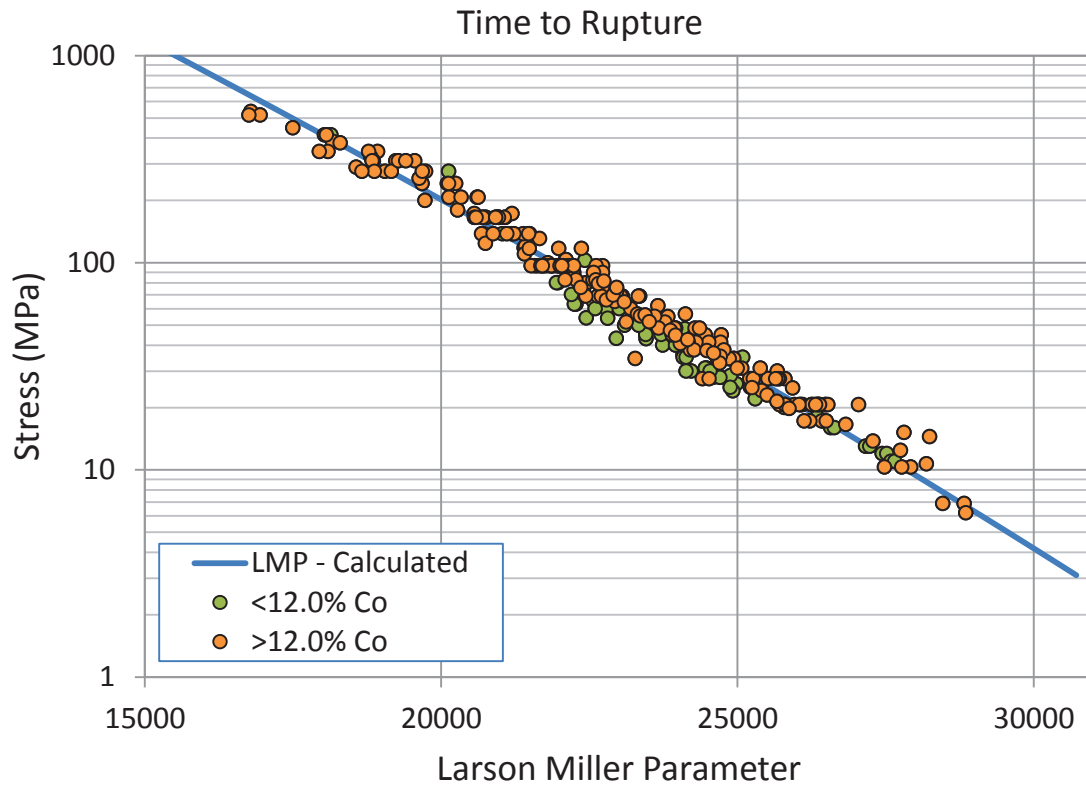


Figure 2. Larson-Miller plot comparing heats with high and low cobalt content.

## 3.2 Time to 1% Strain

A Larson-Miller plot was also created using time to 1% strain rather than creep-rupture time (Figure 3). This value was not reported for all creep-rupture tests, but was available for many of the INL interrupted creep tests, resulting in a data set of 208 specimens. Regression analysis for a linear fit produced a correlation coefficient $R^2 = 0.9272$ and $C = 19.64$ in Equation (1) and $a_0 = 35{,}663$ and $a_1 = -6388.5$ in Equation (2). A linear fit was used rather than a higher order polynomial to prevent the calculated LMP line from curving up, thus ensuring that extrapolation to long time/higher temperature is conservative.

Figure 3. Larson-Miller plot with a linear fit for time to 1% creep strain for Alloy 617.

## 3.3   Time to Onset of Tertiary Creep

A Larson-Miller plot was also created using time to tertiary strain. This value also was not reported for all creep-rupture tests, but was available for many of the INL interrupted creep tests. This data set also contained 208 specimens, although not all the same specimens as the 1% strain data set. Regression analysis for a second order polynomial fit (Figure 4) produced a correlation coefficient $R^2 = 0.9716$, C = 19.05 in Equation (1) and $a_0 = 32,652$ $a_1 = -3178.8$ and $a_2 = -750.00$ in Equation (2). Regression analysis for a linear fit (Figure 5) produced a correlation coefficient $R^2 = 0.9695$ and C = 18.15 in Equation (1) and a0 = 33,545 and $a_1 = -5674.3$ in Equation (2). The linear fit for tertiary stress results in a better fit and higher stress values for larger Larson-Miller parameters, but lower stress values for intermediate Larson-Miller parameters.
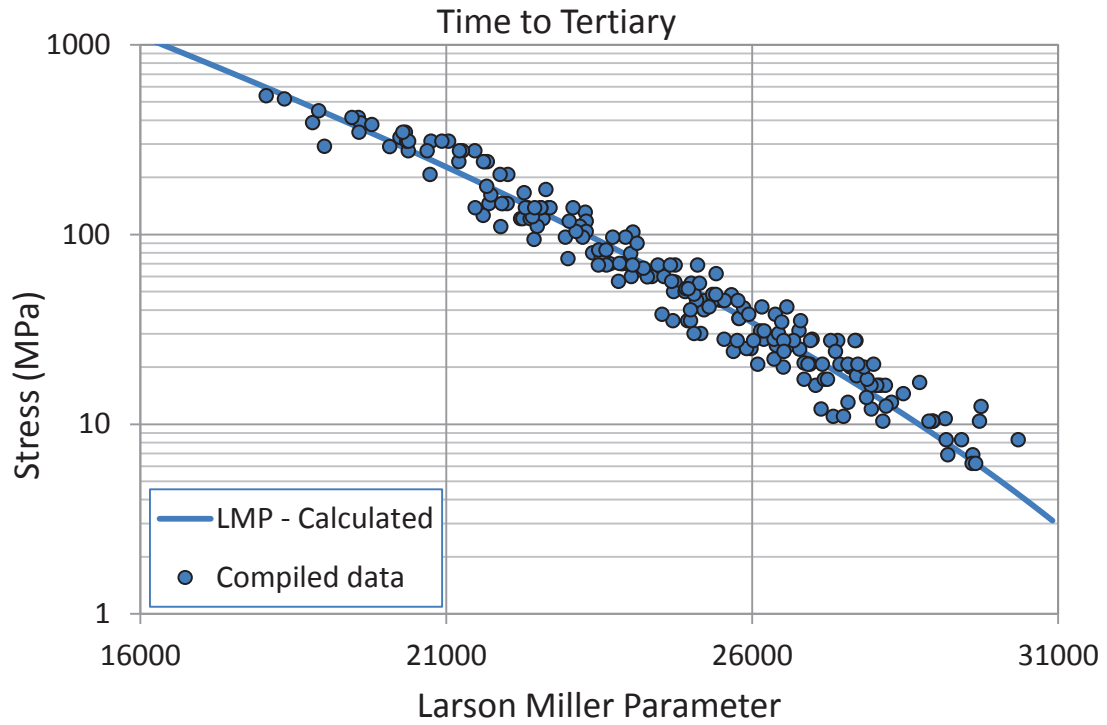
Figure 4. Larson-Miller plot with second-order polynomial fit for time to tertiary creep strain for Alloy 617.
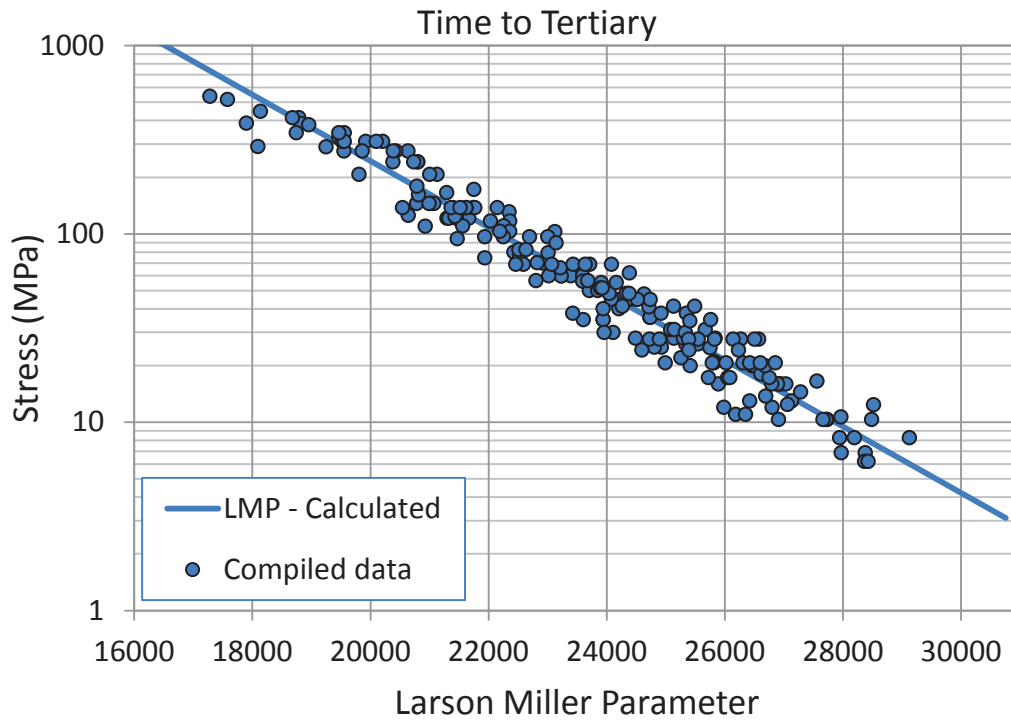


Figure 5. Larson-Miller plot with a linear fit for time to tertiary creep strain for Alloy 617.

# 4.    HOT TENSILE CURVES

Average hot tensile curves are presented along with isochronous stress-strain curves for high temperature nuclear materials in ASME B&PV Section III, Subsection NH-T-1800 [1] for the range of temperatures over which each alloy is qualified for high temperature design. Two models have been examined to describe the elevated temperature plastic tensile behavior of Alloy 617. The Ramberg-Osgood equation describes the shape of the stress strain curves well in the range of 650-800°C, while a modified Voce equation describes the shape for temperatures greater than 800°C. At 800°C, the curves calculated by the two models are nearly identical. Experimental tensile curves from rod and plate tested at INL [16] have been used as the source of stress and strain data (e.g. proportional limit) for fitting purposes, and for determining which model provides the best fit (magnitude and shape of the curve).

To generate a stress-strain curve, the model equation is solved for $e_p$, the engineering plastic strain, and total strain, e, is calculated as:

$$e = 100*S/E + e_p \qquad (4)$$

*where* S is the engineering stress, E is the elastic modulus, and the first term represents elastic strain. The modulus values were taken from the ASME B&PV Code rather than from the experiments.

To obtain minimum hot tensile curves, the modeled curves are shifted along the trajectory of linear elastic deformation in order to pass through $S_y$ at 0.2% offset strain. $S_y$ represents the minimum yield strength and is listed in ASME Section II, Part D, Table Y-1.[2] To obtain an average hot tensile curve, the modeled curves are similarly shifted to pass through $1.25S_y$ at 0.2% offset strain.

## 4.1    Ramberg-Osgood Method

The Ramberg-Osgood equation can be used to model tensile plasticity when creep effects are not significant:

$$e_p = a(S-S_{pl})^m \text{ where } S > S_{pl} \qquad (5)$$

*where* $e_p$ is the engineering plastic strain, S is the engineering stress, $S_{pl}$ is the proportional limit, and a and m are material constants that may vary with strain rate and temperature.[17] The constants a and m are calculated using experimentally determined data pairs $e_p$=0.2% when S=$S_{ys}$ (0.2% offset yield strength), and $e_p$=2% when S=$S_{2\%}$ (2% offset yield strength). The proportional limit and yield strengths were experimentally determined from INL tensile testing on plate material (chemistry listed in Table 1).

## 4.2    Voce Method

A modified Voce equation was used to describe the tensile plasticity:

$$S-S_{UTS} = (S_{pl}-S_{UTS}) \exp [-(b \, e_p)^{0.5}] \qquad (6)$$

*where* S is the engineering stress, $e_p$ is the engineering plastic strain, $S_{UTS}$ is the ultimate tensile strength, $S_{pl}$ is the proportional limit, and b is the rate constant. The latter constant can be calculated when S=$S_{ys}$, yield strength, and ep is 0.2%.[18,19] The proportional limit, yield, and ultimate tensile strengths were experimentally determined from INL tensile testing on plate material (chemistry listed in Table 1).

# 5.    TIME-DEPENDENT STRESS ALLOWABLES

## 5.1    Temperature Limits

Tabulated values of $S_t$ and $S_r$ are required in both conventional (°F, ksi) and metric units. Temperature limits and allowable stresses in the ASME B&PV Code are determined using the conventional units; metric values are determined from the conventional values by calculation or interpolation. This method creates some awkward situations in tabulating values because the temperature limits in conventional and metric units do not coincide. In the allowable stress tables in ASME-Section II-D, for example, a material

might have an upper use temperature limited to 1750°F (954°C). The tabulated values in ASME Section II-D Metric list allowable stresses in 25°C increments. For the case where a material is allowed up to 954°C the process that has been adopted in Section II-D is to provide allowables at 950 and 975°C with a footnote stating: "The maximum use temperature is 954°C; the value listed at 975°C is provided for interpolation purposes only." Section III-NH has not followed the Section II convention. Instead, the values are simply rounded to the nearest standard metric increment. Thus, while Alloy 617 will be allowed up to 1750°F, in metric units its allowed use temperature will be limited to 950°C.

For the current work this has a significant practical advantage. Experimental data are required up to 50°C above the maximum use temperature; because of the rounding to 950°C in Section III-NH it is only necessary to have data to 1000°C which is the upper limit of much of the recent experimental work on Alloy 617.

The lower temperature limit for tabulated values and figures in Section III NH is 800°F. Below this temperature Section III, Subsection NB is used. Current calculations for $S_t$ and $S_r$ have been executed in metric units at 50°C intervals and extend down to 1000°F/600°C, which is approximately the lower limit of available creep data and hot tensile curves. Once lower temperature hot tensile curves are developed, $S_t$ can be extended to 800°F. Calculations at smaller temperature increments and in conventional units will be performed for the Alloy 617 draft Code Case.

## 5.2    Allowable Stress Intensity Values, $S_t$

Both a figure and table must be created for $S_t$ for the Alloy 617 Code Case. An example of the needed values taken from ASME 2013 B&PV Code, Section III, Division 1-NH, Table NH-I-14.4C for Alloy 800H are shown in Figure 6 and Figure 7.
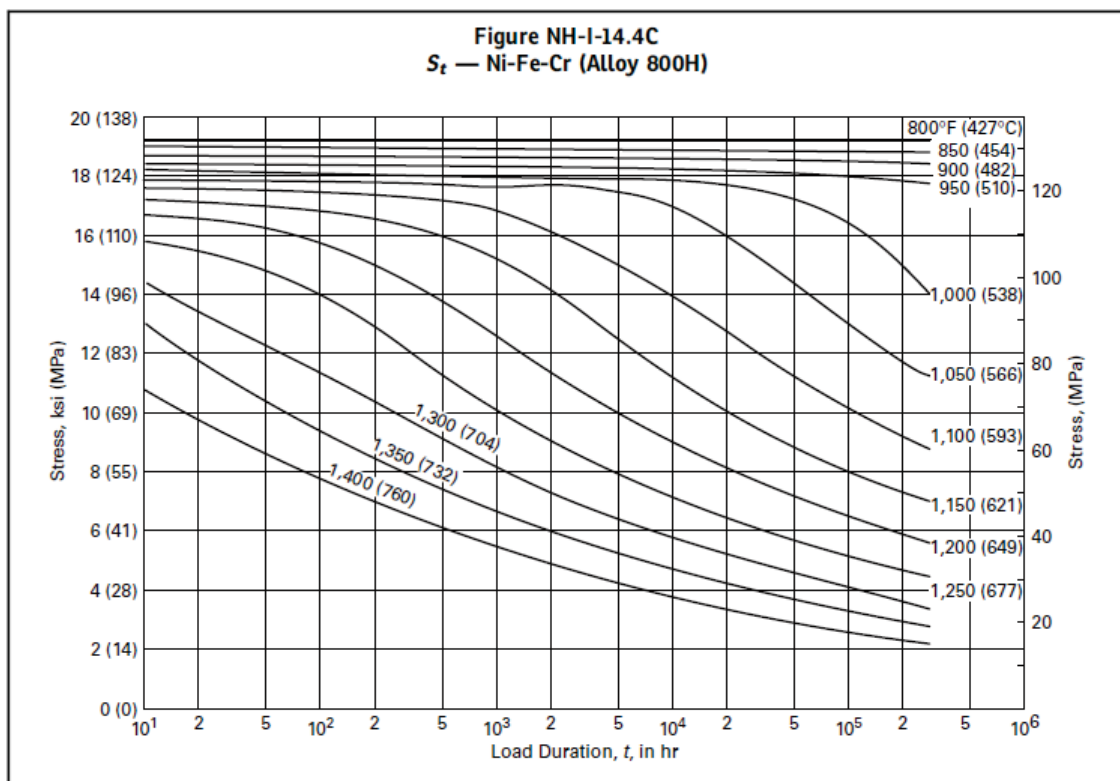


Figure 6. $S_t$ values for Alloy 800 H reproduced from ASME 2013 B&PV Code, Section III, Division 1-NH, Table NH-I-14.4C.

## Table NH-I-14.4C
### $S_t$ — Allowable Stress Intensity Values, ksi (MPa), Ni-Fe-Cr (Alloy 800H)

**U.S. Customary Units**

| Temp., °F | 1 hr | 10 hr | 30 hr | 100 hr | 300 hr | 1,000 hr | 3,000 hr | 10,000 hr | 30,000 hr | 100,000 hr | 300,000 hr |
|---|---|---|---|---|---|---|---|---|---|---|---|
| 800 | 19.2 | 19.2 | 19.2 | 19.2 | 19.2 | 19.2 | 19.2 | 19.2 | 19.2 | 19.1 | 19.1 |
| 850 | 18.9 | 18.9 | 18.9 | 18.9 | 18.9 | 18.9 | 18.9 | 18.9 | 18.9 | 18.8 | 18.8 |
| 900 | 18.7 | 18.7 | 18.7 | 18.7 | 18.7 | 18.7 | 18.6 | 18.6 | 18.6 | 18.5 | 18.4 |
| 950 | 18.4 | 18.4 | 18.4 | 18.4 | 18.4 | 18.4 | 18.3 | 18.2 | 18.2 | 18.0 | 17.8 |
| 1,000 | 18.2 | 18.1 | 18.1 | 18.1 | 18.1 | 18.0 | 17.9 | 17.8 | 17.6 | 16.5 | 14.1 |
| 1,050 | 17.9 | 17.9 | 17.8 | 17.8 | 17.7 | 17.6 | 17.4 | 17.1 | 15.0 | 12.9 | 11.1 |
| 1,100 | 17.6 | 17.6 | 17.5 | 17.4 | 17.2 | 16.9 | 16.3 | 13.9 | 12.0 | 10.3 | 8.9 |
| 1,150 | 17.3 | 17.2 | 17.0 | 16.8 | 16.4 | 15.3 | 13.2 | 11.2 | 9.6 | 8.1 | 7.0 |
| 1,200 | 17.0 | 16.7 | 16.3 | 15.8 | 14.7 | 12.4 | 10.7 | 9.0 | 7.7 | 6.5 | 5.6 |
| 1,250 | 16.5 | 15.8 | 15.2 | 14.1 | 12.0 | 10.1 | 8.6 | 7.2 | 6.2 | 5.2 | 4.4 |
| 1,300 | 15.8 | 14.4 | 13.4 | 11.5 | 9.8 | 8.2 | 7.0 | 5.8 | 5.0 | 4.1 | 3.5 |
| 1,350 | 14.7 | 13.1 | 11.3 | 9.5 | 8.0 | 6.7 | 5.7 | 4.7 | 4.0 | 3.3 | 2.8 |
| 1,400 | 13.0 | 10.8 | 9.3 | 7.8 | 6.5 | 5.4 | 4.6 | 3.8 | 3.2 | 2.6 | 2.2 |

**SI Units**

| Temp., °C | 1 hr | 10 hr | 30 hr | 100 hr | 300 hr | 1,000 hr | 3,000 hr | 10,000 hr | 30,000 hr | 100,000 hr | 300,000 hr |
|---|---|---|---|---|---|---|---|---|---|---|---|
| 425 | 132 | 132 | 132 | 132 | 132 | 132 | 132 | 132 | 132 | 132 | 132 |
| 450 | 130 | 130 | 130 | 130 | 130 | 130 | 130 | 130 | 130 | 130 | 130 |
| 475 | 129 | 129 | 129 | 129 | 129 | 129 | 128 | 128 | 128 | 127 | 126 |
| 500 | 128 | 128 | 128 | 128 | 128 | 128 | 127 | 126 | 126 | 125 | 124 |
| 525 | 126 | 126 | 126 | 126 | 126 | 125 | 124 | 124 | 122 | 119 | 109 |
| 550 | 124 | 124 | 124 | 124 | 124 | 123 | 122 | 121 | 113 | 103 | 88 |
| 575 | 123 | 123 | 123 | 122 | 121 | 120 | 117 | 111 | 96 | 83 | 72 |
| 600 | 121 | 121 | 120 | 119 | 117 | 114 | 107 | 91 | 79 | 67 | 58 |
| 625 | 119 | 118 | 116 | 115 | 109 | 102 | 89 | 75 | 64 | 55 | 47 |
| 650 | 117 | 115 | 112 | 109 | 101 | 85 | 74 | 62 | 53 | 45 | 39 |
| 675 | 114 | 109 | 105 | 98 | 85 | 72 | 61 | 52 | 44 | 37 | 31 |
| 700 | 110 | 100 | 94 | 82 | 70 | 59 | 50 | 41 | 35 | 29 | 25 |
| 725 | 99 | 88 | 82 | 70 | 58 | 49 | 41 | 34 | 29 | 24 | 20 |
| 750 | 94 | 80 | 69 | 58 | 49 | 40 | 34 | 28 | 24 | 20 | 16 |

Figure 7. Stress values for Alloy 800 H reproduced from ASME 2013 B&PV Code, Section III, Division 1-NH, Table NH-I-14.4C.

In order to produce the $S_t$ table required for the code case, each of the three criteria (100% of the average stress required to obtain a total (elastic, plastic, primary and secondary creep) strain of 1%, 67% of the minimum stress to cause rupture, and 80% of the minimum stress to cause the initiation of tertiary creep) must be calculated for the matrix of times and temperatures. This is achieved by using the equations determined by the regression fits of Larson-Miller plots to all acceptable creep data combined with information from the hot tensile curves.

## 5.2.1 Calculating Creep Stress from Larson-Miller Plots

First the LMP is calculated for each time and temperature increment based on Equation (1) using the appropriate C value. To calculate the criteria based on rupture and tertiary creep, the minimum stress is needed rather than the average. This is accomplished by creating a line that is displaced 1.65 standard error of estimate (SEE) in log time from the average stress-to-rupture curve. In order to accomplish this, Equation (1) must be replaced by:

$$LMP = T (C + \log t_R + 1.65\ SEE) \tag{7}$$

SEE is included in the output of the above-mentioned spreadsheet used to calculate and plot the Larson-Miller relationships.

Next the quadratic equation is used to solve for stress, S, in Equation (2) using the appropriate $a_0$, $a_1$ and $a_2$ values (or S is solved directly in the case of a linear fit where $a_2=0$). The rupture stress and tertiary stress levels are reduced to 67% and 80%, respectively.

## 5.2.2 Calculating Total Stress at 1% Strain

As mentioned above, one of the three criteria is 100% of the average stress required to obtain a total (elastic, plastic, primary and secondary creep) strain of 1%. The stress at 1% creep strain is determined from the Larson-Miller plots; however, the stress at 1% plastic + elastic strain must be obtained from the hot tensile curves. The average hot tensile curves are plotted along with isochronous stress-strain curves in ASME B&PV Section III, Subsection NH-T-1800.[1] Table 3 gives stress at 1% plastic strain used as the upper limit for $S_t$. Current practice is to use the minimum hot tensile curves to determine these plastic stress values; although, the average hot tensile curves have been recently used for Type 316 stainless steel after discussion within the ASME Subgroup on Elevated Temperature Design.[20] The Alloy 617 hot tensile curves are under development, so values reported in Table 3 are preliminary. The total stress at a strain of 1% will be the minimum of the elastic/plastic stress from Table 3 and the creep stress from the 1% Larson-Miller plot from Section 3.2 for a given temperature.

Table 3. Stress at 1% plastic strain as a function of temperature obtained from the minimum hot tensile curves.

| Temperature (°C) | Stress (MPa) |
| --- | --- |
| 600 | 193.3 |
| 650 | 193.3 |
| 700 | 192.5 |
| 750 | 193.9 |
| 800 | 181.3 |
| 850 | 159.2 |
| 900 | 129.3 |
| 950 | 110.5 |
| 1000 | 83.4 |

## 5.2.3 Determining $S_t$

To determine $S_t$ the minimum of the three criteria is determined for each time/temperature combination. The stress values calculated for each criterion are shown in Table 4. The values reported for time to tertiary creep are based on the second order Larson-Miller regression fit. Table 5 presents the $S_t$ (minimum) value for three different methods of treating tertiary creep: a first order regression fit, a second order regression fit, and elimination of tertiary creep as one of the criteria. Colors are used to illustrate which criterion is governing for each time/temperature combination. As expected from the Larson-Miller plots shown in Figure 4 and Figure 5, the linear fit for tertiary stress results in higher stress values for some high-temperature/long-time combinations, but lower stress values for many other combinations (Figure 8). Analysis of tertiary creep influence on $S_t$ is presented here for completeness. The ASME Section III Working Group on Allowable Stress Criteria has suggested that this criterion is not appropriate for Alloy 617. The arguments for eliminating the tertiary creep criterion and supporting microstructural evidence are presented in an appendix. When the tertiary creep criterion is not used, rupture governs the creep behavior in all cases; the 1% total strain criterion is only governing when the behavior is primarily plastic (little or no creep). $S_t$ is increased over a wide range of time and temperatures by eliminating the tertiary creep criterion, as shown in Figure 9.

Table 4. Calculated stress criteria used to determine $S_t$ values.

| Time (h)→ | 1 | 3 | 10 | 30 | 100 | 300 | 1000 | 3000 | 10000 | 30000 | 100000 |
|---|---|---|---|---|---|---|---|---|---|---|---|
| | | | | | | Stress (MPa) | | | | | |
| Temperature (°C) ↓ | | | | | 67% Minimum $S_r$ | | | | | | |
| 600 | 624.5 | 539.8 | 459.8 | 396.9 | 337.6 | 291.1 | 247.2 | 212.8 | 180.5 | 155.2 | 131.4 |
| 650 | 455.5 | 389.9 | 328.5 | 280.8 | 236.2 | 201.6 | 169.3 | 144.2 | 120.9 | 102.9 | 86.1 |
| 700 | 331.2 | 280.7 | 233.9 | 197.9 | 164.6 | 139.0 | 115.4 | 97.3 | 80.6 | 67.8 | 56.1 |
| 750 | 240.2 | 201.5 | 166.0 | 139.0 | 114.3 | 95.5 | 78.4 | 65.3 | 53.5 | 44.5 | 36.3 |
| 800 | 173.6 | 144.1 | 117.4 | 97.3 | 79.0 | 65.3 | 52.9 | 43.7 | 35.3 | 29.0 | 23.4 |
| 850 | 125.1 | 102.7 | 82.7 | 67.8 | 54.4 | 44.5 | 35.6 | 29.0 | 23.2 | 18.8 | 15.0 |
| 900 | 89.8 | 73.0 | 58.1 | 47.0 | 37.3 | 30.1 | 23.8 | 19.2 | 15.1 | 12.1 | 9.5 |
| 950 | 64.3 | 51.7 | 40.6 | 32.5 | 25.5 | 20.3 | 15.9 | 12.6 | 9.8 | 7.8 | 6.0 |
| Temperature (C) ↓ | | | | | Average $S_{1\%}$ | | | | | | |
| 600 | 193.3 | 193.3 | 193.3 | 193.3 | 193.3 | 193.3 | 193.3 | 193.3 | 193.3 | 193.3 | 164.0 |
| 650 | 193.3 | 193.3 | 193.3 | 193.3 | 193.3 | 193.3 | 193.3 | 174.6 | 146.7 | 125.2 | 105.2 |
| 700 | 192.5 | 192.5 | 192.5 | 192.5 | 192.5 | 163.4 | 136.0 | 115.1 | 95.8 | 81.0 | 67.5 |
| 750 | 193.9 | 193.9 | 189.1 | 158.6 | 130.8 | 109.7 | 90.5 | 75.9 | 62.6 | 52.5 | 43.3 |
| 800 | 181.3 | 159.6 | 130.4 | 108.4 | 88.6 | 73.6 | 60.2 | 50.0 | 40.9 | 34.0 | 27.8 |
| 850 | 134.7 | 111.0 | 89.9 | 74.1 | 60.0 | 49.4 | 40.0 | 33.0 | 26.7 | 22.0 | 17.8 |
| 900 | 94.5 | 77.3 | 61.9 | 50.6 | 40.6 | 33.2 | 26.6 | 21.7 | 17.4 | 14.2 | 11.4 |
| 950 | 66.4 | 53.8 | 42.7 | 34.6 | 27.5 | 22.3 | 17.7 | 14.3 | 11.4 | 9.2 | 7.3 |
| Temperature (C) ↓ | | | | 80% Minimum $S_{tertiary}$ (Second Order Fit) | | | | | | | |
| 600 | 589.0 | 517.7 | 448.7 | 393.2 | 339.6 | 296.5 | 255.1 | 221.9 | 190.1 | 164.7 | 140.5 |
| 650 | 431.7 | 375.3 | 321.1 | 278.0 | 236.9 | 204.2 | 173.2 | 148.6 | 125.4 | 107.0 | 89.8 |
| 700 | 313.7 | 269.4 | 227.4 | 194.4 | 163.2 | 138.7 | 115.8 | 97.9 | 81.2 | 68.2 | 56.1 |
| 750 | 225.7 | 191.3 | 159.1 | 134.1 | 110.8 | 92.8 | 76.1 | 63.3 | 51.5 | 42.4 | 34.2 |
| 800 | 160.7 | 134.3 | 109.9 | 91.3 | 74.1 | 61.0 | 49.1 | 40.0 | 31.8 | 25.7 | 20.2 |
| 850 | 113.1 | 93.1 | 74.9 | 61.1 | 48.6 | 39.3 | 30.9 | 24.7 | 19.2 | 15.1 | 11.5 |
| 900 | 78.5 | 63.6 | 50.1 | 40.2 | 31.3 | 24.7 | 19.0 | 14.8 | 11.1 | 8.5 | 6.3 |
| 950 | 53.8 | 42.7 | 33.0 | 25.8 | 19.6 | 15.1 | 11.3 | 8.5 | 6.2 | 4.6 | 3.2 |

Table 5. Minimum value used to determine $S_t$, both with and without the tertiary creep criterion. Colors are used to illustrate which criterion is governing for each time/temperature combination.

| | Stress (MPa) | | | | | | | | | | |
|---|---|---|---|---|---|---|---|---|---|---|---|
| Time (h)→ | 1 | 3 | 10 | 30 | 100 | 300 | 1000 | 3000 | 10000 | 30000 | 100000 |
| Temperature (C) ↓ | Minimum, All Criteria, Second Order Tertiary | | | | | | | | | | |
| 600 | 193.3 | 193.3 | 193.3 | 193.3 | 193.3 | 193.3 | 193.3 | 193.3 | 180.5 | 155.2 | 131.4 |
| 650 | 193.3 | 193.3 | 193.3 | 193.3 | 193.3 | 193.3 | 169.3 | 144.2 | 120.9 | 102.9 | 86.1 |
| 700 | 192.5 | 192.5 | 192.5 | 192.5 | 163.2 | 138.7 | 115.4 | 97.3 | 80.6 | 67.8 | 56.1 |
| 750 | 193.9 | 191.3 | 159.1 | 134.1 | 110.8 | 92.8 | 76.1 | 63.3 | 51.5 | 42.4 | 34.2 |
| 800 | 160.7 | 134.3 | 109.9 | 91.3 | 74.1 | 61.0 | 49.1 | 40.0 | 31.8 | 25.7 | 20.2 |
| 850 | 113.1 | 93.1 | 74.9 | 61.1 | 48.6 | 39.3 | 30.9 | 24.7 | 19.2 | 15.1 | 11.5 |
| 900 | 78.5 | 63.6 | 50.1 | 40.2 | 31.3 | 24.7 | 19.0 | 14.8 | 11.1 | 8.5 | 6.3 |
| 950 | 53.8 | 42.7 | 33.0 | 25.8 | 19.6 | 15.1 | 11.3 | 8.5 | 6.2 | 4.6 | 3.2 |
| Temperature (C) ↓ | Minimum, All Criteria, Linear Tertiary | | | | | | | | | | |
| 600 | 193.3 | 193.3 | 193.3 | 193.3 | 193.3 | 193.3 | 193.3 | 193.3 | 180.5 | 155.2 | 131.4 |
| 650 | 193.3 | 193.3 | 193.3 | 193.3 | 193.3 | 193.3 | 169.3 | 144.2 | 118.7 | 99.3 | 81.6 |
| 700 | 192.5 | 192.5 | 192.5 | 192.5 | 164.0 | 135.8 | 110.5 | 91.5 | 74.4 | 61.7 | 50.2 |
| 750 | 193.9 | 193.9 | 162.2 | 133.0 | 107.1 | 87.8 | 70.7 | 58.0 | 46.7 | 38.3 | 30.8 |
| 800 | 167.1 | 135.7 | 108.1 | 87.8 | 69.9 | 56.8 | 45.3 | 36.8 | 29.3 | 23.8 | 18.9 |
| 850 | 113.6 | 91.4 | 72.1 | 58.0 | 45.7 | 36.8 | 29.0 | 23.3 | 18.4 | 14.8 | 11.6 |
| 900 | 77.3 | 61.6 | 48.0 | 38.3 | 29.8 | 23.8 | 18.5 | 14.8 | 11.5 | 9.2 | 7.2 |
| 950 | 52.6 | 41.5 | 32.0 | 25.3 | 19.5 | 15.4 | 11.9 | 9.4 | 7.2 | 5.7 | 4.4 |
| Temperature (C) ↓ | Minimum Without Tertiary | | | | | | | | | | |
| 600 | 193.3 | 193.3 | 193.3 | 193.3 | 193.3 | 193.3 | 193.3 | 193.3 | 180.5 | 155.2 | 131.4 |
| 650 | 193.3 | 193.3 | 193.3 | 193.3 | 193.3 | 193.3 | 169.3 | 144.2 | 120.9 | 102.9 | 86.1 |
| 700 | 192.5 | 192.5 | 192.5 | 192.5 | 164.6 | 139.0 | 115.4 | 97.3 | 80.6 | 67.8 | 56.1 |
| 750 | 193.9 | 193.9 | 166.0 | 139.0 | 114.3 | 95.5 | 78.3 | 65.3 | 53.5 | 44.5 | 36.3 |
| 800 | 173.6 | 144.1 | 117.4 | 97.2 | 79.0 | 65.3 | 52.9 | 43.6 | 35.3 | 29.0 | 23.4 |
| 850 | 125.1 | 102.7 | 82.7 | 67.8 | 54.4 | 44.5 | 35.6 | 29.0 | 23.2 | 18.8 | 15.0 |
| 900 | 89.8 | 73.0 | 58.0 | 47.0 | 37.3 | 30.1 | 23.8 | 19.2 | 15.1 | 12.1 | 9.5 |
| 950 | 64.3 | 51.7 | 40.6 | 32.5 | 25.5 | 20.3 | 15.9 | 12.6 | 9.8 | 7.8 | 6.0 |

14
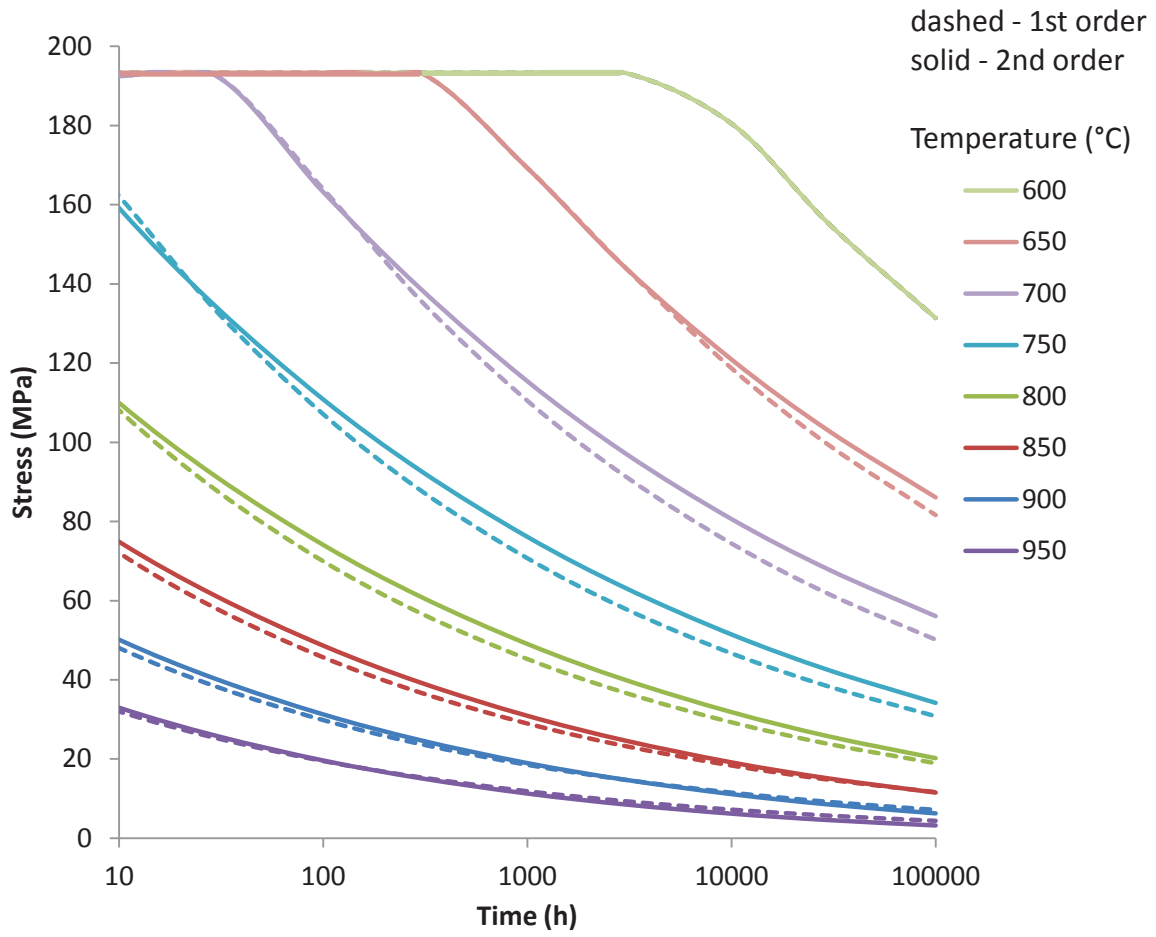
Figure 8. Comparison of $S_t$ as a function of time, calculated using first-order versus second-order polynomial fits to Larson-Miller plots for onset of tertiary creep.
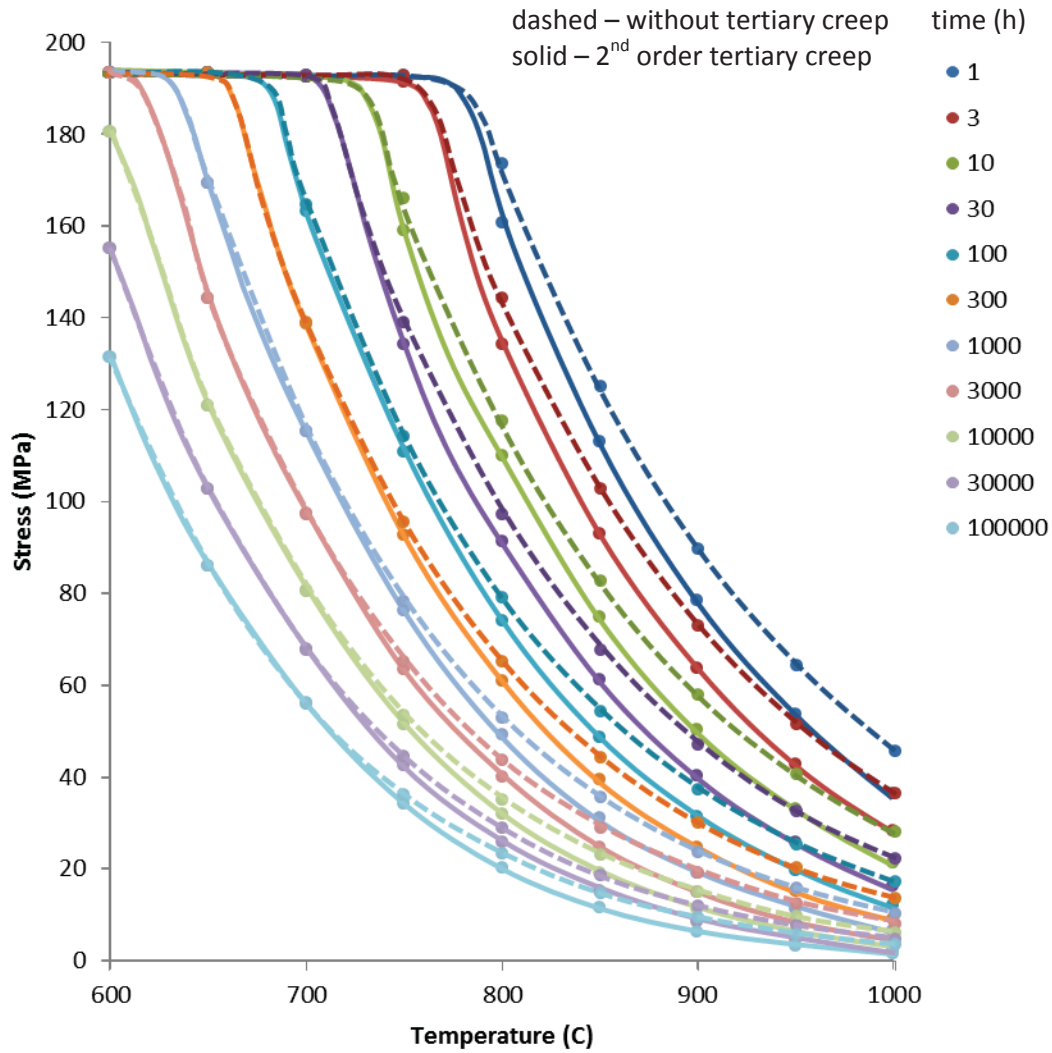
Figure 9. Comparison of $S_t$ calculated using second-order polynomial fit to Larson-Miller plots for onset of tertiary creep, and without tertiary creep criterion, plotted as a function of temperature.

The $S_t$ values calculated in this study are compared to values given in the draft Code Case developed in the early 1990's by Corum and Blass [17] as a function of time in Figure 10. This required conversion of the calculated values from metric to conventional units, since Corum and Blass only presented $S_t$ in conventional units. One of the primary differences between the sets of curves results from using much higher stress values for 1% plastic strain, which determines the stress level of the plateau at lower temperatures. The curves are similar to each other at high temperatures and long times.
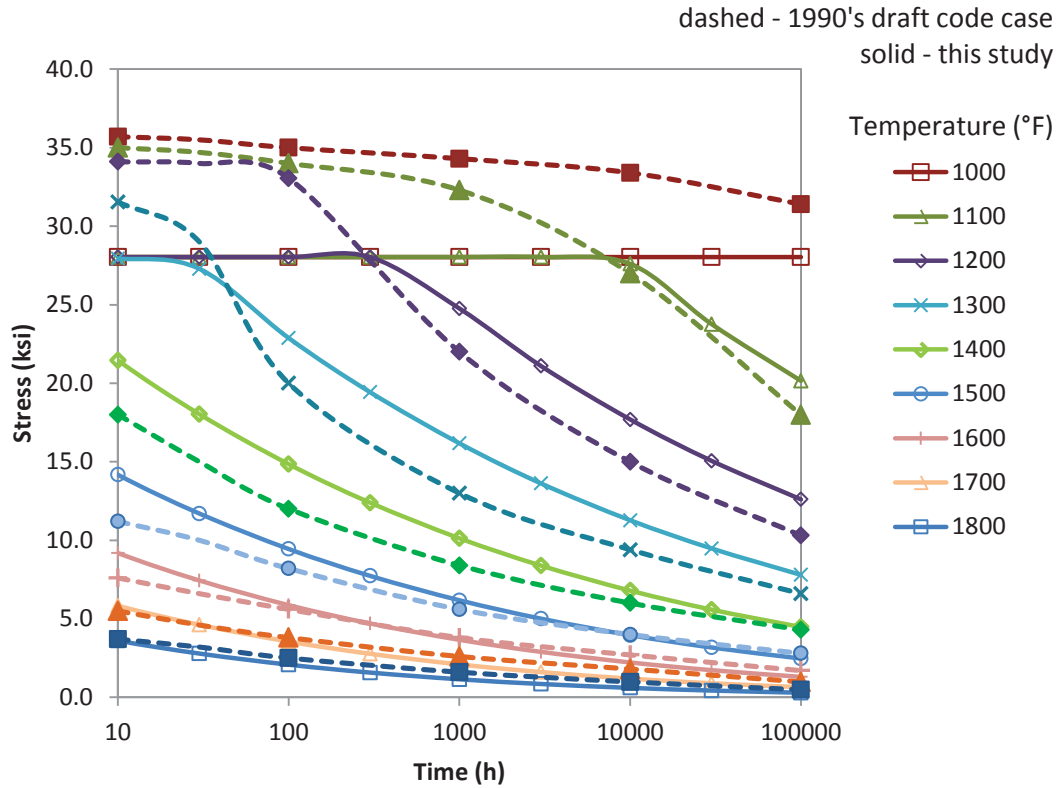
Figure 10. Calculated $S_t$ as a function of time compared to values given in the draft Code Case developed in the early 1990s by Corum and Blass.

## 5.3   Expected Minimum Stress to Rupture, $S_r$

Both a figure and table must be created for Minimum Stress-to-Rupture, $S_r$, for the Alloy 617 Code Case.  An example of the needed values taken from the ASME 2013 B&PV Code, Section III, Division 1 – NH [1] for Alloy 800H are shown in Figure 11 and Figure 12.

Figure 11. Figure of $S_r$ values for Alloy 800 H reproduced from the ASME 2013 B&PV Code, Section III, Division 1 – NH.

18

## Table NH-I-14.6C
### Expected Minimum Stress-to-Rupture Values, ksi (MPa), Ni-Fe-Cr (Alloy 800H)

**U.S. Customary Units**

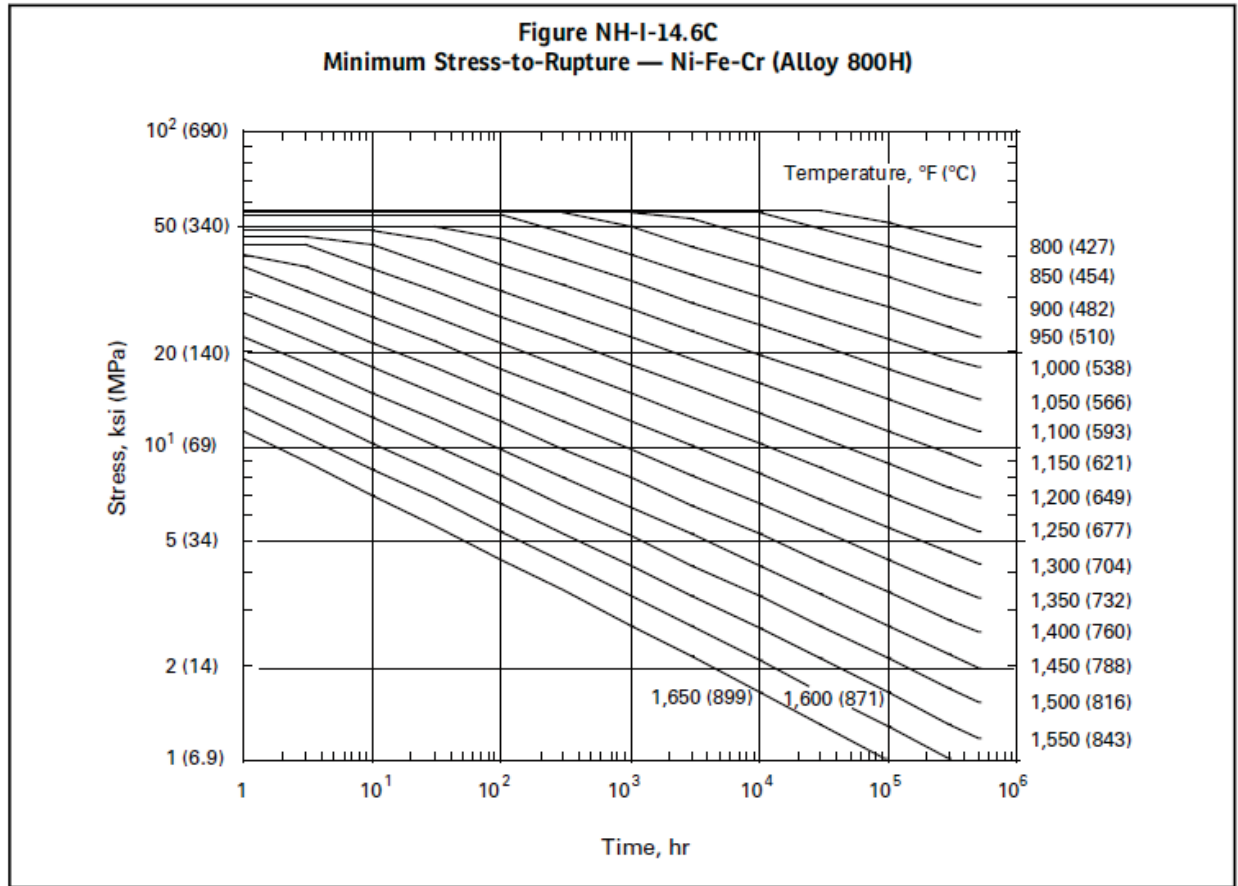| Temp., °F | 1 hr | 3 hr | 10 hr | 30 hr | 100 hr | 300 hr | 1,000 hr | 3,000 hr | 10,000 hr | 30,000 hr | 100,000 hr | 300,000 hr | 500,000 hr |
|---|---|---|---|---|---|---|---|---|---|---|---|---|---|
| 800 | 56.2 | 56.2 | 56.2 | 56.2 | 56.2 | 56.2 | 56.2 | 56.2 | 56.2 | 56.2 | 51.9 | 45.9 | 43.3 |
| 850 | 55.9 | 55.9 | 55.9 | 55.9 | 55.9 | 55.9 | 55.9 | 55.9 | 55.9 | 49.6 | 43.0 | 37.8 | 35.6 |
| 900 | 55.6 | 55.6 | 55.6 | 55.6 | 55.6 | 55.6 | 55.6 | 53.0 | 45.8 | 40.1 | 34.5 | 30.2 | 28.3 |
| 950 | 55.3 | 55.3 | 55.3 | 55.3 | 55.3 | 55.3 | 49.8 | 43.4 | 37.2 | 32.3 | 27.7 | 24.0 | 22.5 |
| 1,000 | 54.7 | 54.7 | 54.7 | 54.7 | 54.7 | 47.9 | 40.9 | 35.4 | 30.1 | 26.0 | 22.1 | 19.1 | 17.8 |
| 1,050 | 50.2 | 50.2 | 50.2 | 50.2 | 45.9 | 39.5 | 33.5 | 28.8 | 24.4 | 20.9 | 17.7 | 15.1 | 14.1 |
| 1,100 | 48.4 | 48.4 | 48.4 | 45.0 | 38.0 | 32.5 | 27.4 | 23.4 | 19.7 | 16.8 | 14.1 | 12.0 | 11.1 |
| 1,150 | 46.3 | 46.3 | 44.0 | 37.5 | 31.5 | 26.8 | 22.4 | 19.0 | 15.9 | 13.4 | 11.2 | 9.5 | 8.7 |
| 1,200 | 43.9 | 43.9 | 36.8 | 31.2 | 26.0 | 22.0 | 18.3 | 15.4 | 12.8 | 10.7 | 8.9 | 7.5 | 6.9 |
| 1,250 | 41.1 | 37.1 | 30.8 | 25.9 | 21.5 | 18.0 | 14.9 | 12.5 | 10.3 | 8.6 | 7.0 | 5.9 | 5.4 |
| 1,300 | 37.2 | 31.2 | 25.7 | 21.5 | 17.7 | 14.8 | 12.1 | 10.1 | 8.2 | 6.8 | 5.6 | 4.6 | 4.2 |
| 1,350 | 31.4 | 26.2 | 21.5 | 17.8 | 14.6 | 12.1 | 9.8 | 8.1 | 6.6 | 5.4 | 4.4 | 3.6 | 3.3 |
| 1,400 | 26.5 | 22.0 | 17.9 | 14.8 | 12.0 | 9.9 | 8.0 | 6.5 | 5.3 | 4.3 | 3.4 | 2.8 | 2.6 |
| 1,450 | 22.4 | 18.4 | 14.9 | 12.2 | 9.8 | 8.0 | 6.4 | 5.2 | 4.2 | 3.4 | 2.7 | 2.2 | 2.0 |
| 1,500 | 18.9 | 15.4 | 12.4 | 10.1 | 8.0 | 6.5 | 5.2 | 4.2 | 3.3 | 2.7 | 2.1 | 1.7 | 1.5 |
| 1,550 | 15.9 | 12.9 | 10.3 | 8.3 | 6.6 | 5.3 | 4.2 | 3.4 | 2.6 | 2.1 | 1.6 | 1.3 | 1.2 |
| 1,600 | 13.3 | 10.8 | 8.5 | 6.8 | 5.4 | 4.3 | 3.4 | 2.7 | 2.1 | 1.7 | 1.3 | 1.0 | 0.91 |
| 1,650 | 11.2 | 9.0 | 7.0 | 5.6 | 4.4 | 3.5 | 2.7 | 2.1 | 1.6 | 1.3 | 1.0 | 0.78 | 0.70 |

**SI Units**

| Temp., °C | 1 hr | 3 hr | 10 hr | 30 hr | 100 hr | 300 hr | 1,000 hr | 3,000 hr | 10,000 hr | 30,000 hr | 100,000 hr | 300,000 hr | 500,000 hr |
|---|---|---|---|---|---|---|---|---|---|---|---|---|---|
| 425 | 387 | 387 | 387 | 387 | 387 | 387 | 387 | 387 | 387 | 387 | 374 | 330 | 312 |
| 450 | 385 | 385 | 385 | 385 | 385 | 385 | 385 | 385 | 385 | 354 | 307 | 270 | 254 |
| 475 | 384 | 384 | 384 | 384 | 384 | 384 | 384 | 384 | 333 | 292 | 252 | 220 | 207 |
| 500 | 382 | 382 | 382 | 382 | 382 | 382 | 369 | 321 | 276 | 241 | 207 | 180 | 168 |
| 525 | 379 | 379 | 379 | 379 | 379 | 361 | 309 | 268 | 229 | 198 | 169 | 146 | 137 |
| 550 | 352 | 352 | 352 | 352 | 351 | 303 | 258 | 223 | 189 | 163 | 138 | 119 | 111 |
| 575 | 342 | 342 | 342 | 342 | 297 | 255 | 216 | 185 | 156 | 134 | 113 | 96 | 90 |
| 600 | 331 | 331 | 331 | 297 | 250 | 214 | 180 | 154 | 129 | 110 | 92 | 78 | 72 |
| 625 | 317 | 317 | 296 | 252 | 211 | 180 | 150 | 127 | 106 | 90 | 75 | 63 | 58 |
| 650 | 302 | 302 | 252 | 214 | 178 | 150 | 125 | 105 | 87 | 73 | 61 | 51 | 47 |
| 675 | 285 | 259 | 215 | 181 | 150 | 126 | 104 | 87 | 72 | 60 | 49 | 41 | 38 |
| 700 | 264 | 221 | 183 | 153 | 126 | 105 | 86 | 72 | 59 | 49 | 40 | 33 | 30 |
| 725 | 227 | 189 | 155 | 129 | 106 | 88 | 71 | 59 | 48 | 40 | 32 | 26 | 24 |
| 750 | 195 | 162 | 132 | 109 | 89 | 73 | 59 | 49 | 39 | 32 | 26 | 21 | 19 |
| 775 | 167 | 138 | 112 | 92 | 74 | 61 | 49 | 40 | 32 | 26 | 21 | 17 | 15 |
| 800 | 143 | 118 | 95 | 77 | 62 | 51 | 40 | 33 | 26 | 21 | 17 | 13 | 12 |
| 825 | 123 | 100 | 80 | 65 | 52 | 42 | 33 | 27 | 21 | 17 | 13 | 11 | 9.7 |
| 850 | 105 | 85 | 68 | 55 | 43 | 35 | 27 | 22 | 17 | 14 | 11 | 8.5 | 7.6 |
| 875 | 90 | 72 | 57 | 46 | 36 | 29 | 23 | 18 | 14 | 11 | 8.5 | 6.7 | 6.0 |
| 900 | 77 | 61 | 48 | 38 | 30 | 24 | 18 | 15 | 11 | 8.9 | 6.8 | 5.3 | 4.7 |

Figure 12. Table of $S_r$ values for Alloy 800 H reproduced from the ASME 2013 B&PV Code, Section III, Division 1 – NH.

The minimum stress to rupture is calculated from the Larson-Miller relationship for rupture (Figure 1) according to Equation (7), as described in Section 5.2.1. For $S_r$ the 67% reduction that was applied when determining the stress-rupture criterion for $S_t$ is not required. The upper bound on the $S_r$ values is controlled by the ultimate strength and has been set at $S_u/1.1$ following the procedure recently applied to Types 304 and 316 stainless steel.[20] $S_u$ is the ultimate strength of the material and can be found for Alloy 617 in Table U in ASME B&PV Section II, Part D [2] up to 525°C. Higher temperature values for materials approved for use in elevated temperature nuclear applications appear in Table NH-3225-1, of Section III, NH [1]. The values proposed for Alloy 617 are shown in Table 6. The values of $S_r$ are shown in Table 7 and plotted in Figure 13. Orange is used in Table 7 to illustrate which time/temperature

combinations are governed by time-dependent behavior (creep); white cells are governed by the ultimate tensile strength.

Table 6. Ultimate strength proposed for Alloy 617 as a function of temperature.

| T (°C) | $S_u$ (MPa) | $S_u/1.1$ (MPa) |
|---|---|---|
| 600 | 570 | 518.2 |
| 650 | 534 | 485.5 |
| 700 | 487 | 442.7 |
| 750 | 428 | 389.1 |
| 800 | 359 | 326.4 |
| 850 | 284 | 258.2 |
| 900 | 208 | 189.1 |
| 950 | 139 | 126.4 |

Table 7. $S_r$, Minimum Stress-to-Rupture Values, in SI.

| | Stress (MPa) | | | | | | | | | | |
|---|---|---|---|---|---|---|---|---|---|---|---|
| Time (h)→ | 1 | 3 | 10 | 30 | 100 | 300 | 1000 | 3000 | 10000 | 30000 | 100000 |
| Temperature (°C) ↓ | | | | | | Minimum $S_r$ | | | | | |
| 600 | 518 | 518 | 518 | 518 | 503 | 434 | 369 | 317 | 269 | 231 | 196 |
| 650 | 485 | 485 | 485 | 419 | 352 | 300 | 252 | 215 | 180 | 153 | 128 |
| 700 | 443 | 418 | 349 | 295 | 245 | 207 | 172 | 145 | 120 | 101 | 84 |
| 750 | 358 | 300 | 247 | 207 | 170 | 142 | 117 | 97 | 80 | 66 | 54 |
| 800 | 259 | 215 | 175 | 145 | 118 | 97 | 79 | 65 | 53 | 43 | 35 |
| 850 | 186 | 153 | 123 | 101 | 81 | 66 | 53 | 43 | 35 | 28 | 22 |
| 900 | 134 | 109 | 87 | 70 | 56 | 45 | 36 | 29 | 23 | 18 | 14 |
| 950 | 96 | 77 | 61 | 48 | 38 | 30 | 24 | 19 | 15 | 12 | 9 |
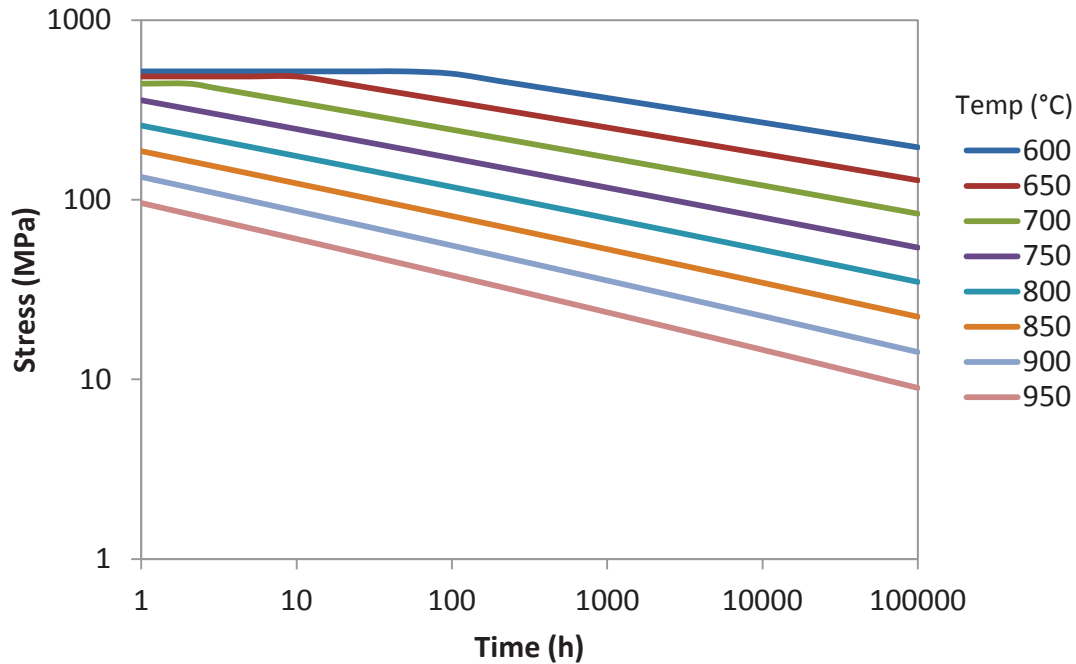
Figure 13. $S_r$ vs. time for 600-950°C in SI units.

# 6. CONCLUSIONS

Time-dependent allowable stresses have been determined using the criteria in Section III-NH of the ASME B&PV Code. $S_t$ is defined as the lesser of three quantities: 100% of the average stress required to obtain a total (elastic, plastic, primary and secondary creep) strain of 1%, 67% of the minimum stress to cause rupture, and 80% of the minimum stress to cause the initiation of tertiary creep. The values are reported for a range of temperatures and for time increments up to 100,000 hours. These values are determined from uniaxial creep tests, which involve the elevated temperature application of a constant load which is relatively small, resulting in deformation over a long time period prior to rupture. The stress which is the minimum resulting from these criteria is the time-dependent allowable stress $S_t$. Values of minimum stress to cause rupture, $S_r$, calculated as part of the $S_t$ determination, are also reported.

Data from a large number of creep and creep-rupture tests on Alloy 617 are analyzed using the ASME Section III-NH criteria. Data which are used in the analysis are from the ongoing Department of Energy sponsored high-temperature materials program, from KAERI through the GIF VHTR Materials Program and historical data from previous high-temperature reactor research and vendor data generated in developing the alloy.

It is found that the tertiary creep criterion determines $S_t$ at highest temperatures, while the stress to cause 1% total strain controls at low temperatures. The ASME Section III Working Group on Allowable Stress Criteria has recommended that the uncertainties associated with determining the onset of tertiary creep and the lack of significant cavitation associated with early tertiary creep strain suggest that the tertiary creep criteria is not appropriate for this material. If the tertiary creep criterion is dropped from consideration, the stress to rupture criteria determines $S_t$ at all but the lowest temperatures.

# 7.  REFERENCES

1  ASME International, Boiler and Pressure Vessel Code, Section III, "Rules for Construction of Nuclear Facility Components," Division 1 — Subsection NH, Class 1 Components in Elevated Temperature Service, 2013.

2  ASME International, Boiler and Pressure Vessel Code, Section II, "Materials," Part D, Properties (Customary), 2013.

3  ASTM International, "E139-06 Standard Test Methods for Conducting Creep, Creep-Rupture, and Stress-Rupture Tests of Metallic Materials," 2006.

4  Weiju, R., 2009, "Gen IV Materials Handbook Functionalities and Operation," ORNL/TM-2009/285, U.S. Department of Energy Office of Nuclear Energy, December 2, 2009.

5  K. Natesan, M. Li, W. K. Soppet, and D. L. Rink, "Creep Testing of Alloy 617 and A508/533 Base metals and Weldments," Argonne National Laboratory, ANL/EXT-12/36, Sep. 2012.

6  W. G. Kim, S. N. Yin, G.-G. Lee, and Y.-W. Kim, "Creep Behavior for Alloy 617 in Air at 950 C," *Mater. Sci. Forum*, vol. 654–656, pp. 508–511, 2010.

7  W.-G. Kim, Song-Nan Yin, Y.-W. Kim, and W.-S. Ryu, "Creep behaviour and long-term creep life extrapolation of alloy 617 for a very high temperature gas-cooled reactor," Trans. Indian Inst. Met., vol. 63, no. 2–3, pp. 145–150, 2010.

8  W.-G. Kim, I. M. W. Ekaputra, J.-Y. Park, M.-H. Kim, and Y.-W. Kim, "Investigation of Creep Rupture Properties in Air and He Environments of Alloy 617 at 800 C," in *Proceedings of HTR 2014*, Weihai, China, 2014.

9  W.-G. Kim, S.-N. Yin, G.-G. Lee, Y.-W. Kim, and Seon-Jin Kim, "Creep oxidation behaviour and creep strength prediction for Alloy 617," *Int. J. Press. Vessels Pip*., vol. 87, pp. 289–295, 2010.

10  ASTM International, E139-11, "Standard Test methods for Conducting Creep, Creep-Rupture, and Stress-Rupture Tests of Metallic Materials, 2006.

11  Cook, "Creep Properties of INCONEL-617 in Air and Helium at 800 to 1000 C," *Nucl. Technol*., vol. 66, pp. 283–288, 1984.

12  S. Chomette, J. M. Gentzbittel, and B. Viguier, "Creep behaviour of as received, aged and cold worked INCONEL 617 at 850°C and 950°C," *J. Nucl. Mater.*, vol. 399, no. 2–3, pp. 266–274

13  F. R. Larson and J. Miller, "A Time-Temperature Relationship for Rupture and Creep Stresses," *Trans. ASME*, vol. 74, p. 765−775, 1952.

14  L. H. Sjodahl, "A Comprehensive Method of Rupture Data Analysis With Simplified Models," in *Characterization of Materials for Service at Elevated Temperatures*, New York, NY: American Society of Mechanical Engineers, 1978, pp. 501–516.

15  R. W. Swindeman and M. J. Swindeman, *Analysis of Time-Dependent Materials Properties Data.* ASME Standards Technology, LLC, 2014.

16  J. K. Wright, L. J. Carroll, C. Cabet, T. M. Lillo, J. K. Benz, J. A. Simpson, W. R. Lloyd, J. A. Chapman, and R. N. Wright, "Characterization of elevated temperature properties of heat exchanger and steam generator alloys," *Nucl. Eng. Des.*, vol. 251, pp. 252–260, 2012.

17  J. M. Corum and J. J. Blass, "Rules for Design of Alloy 617 Nuclear Components to Very High Temperatures," *PVP Press. Vessel Pip. Fatigue Fract. Risk ASME*, vol. 215, pp. 147–153, 1991.

18  E. Voce, "The Relationship Between Stress and Strain for Homogeneous Deformation," *J. Inst. Met.*, vol. 74, p. 537, 1948.

19  R. W. Swindeman, "Construction of isochronous stress-strain curvves for 9Cr-1Mo-V steel," *PVP Press. Vessel Pip. Adv. Life Predict. Methodol. ASME*, vol. 391, pp. 95–100, 1999.

20  M. Sengupta and J. E. Nestell, MPR-3813, Revision 2, "Task 14a – Correct and Extend Allowable Stress Values for 304 and 316 Stainless Steel," ASME Standards Technology, LLC, October, 2013.

# Appendix A

# Tertiary Creep

# Appendix A

# Tertiary Creep

Incorporation of a tertiary creep criterion in ASME B&PV Section III, Division 1 Subsection NH, for estimating the time-dependent allowable stress value, $S_t$, is based on the behavior of austenitic stainless steels where primary and secondary creep represent the majority of the creep life of the material while tertiary creep is relatively short. The tertiary creep criterion was adopted after it was observed experimentally that internally pressurized tubes of austenitic stainless steel leaked due to creep damage at times less than those predicted using analysis based on uniaxial rupture data. In the absence of extensive experimental tube failure data over a range of relevant temperatures, this criterion was developed based on the logic that the onset of tertiary creep during uniaxial testing of austenitic stainless steels is associated with extensive creep induced cavitation. Eliminating tertiary creep, and the associated cavitation, was presumed to represent a conservative indirect limit to minimize the potential for premature failure of tubes under multi-axial loading. Although Alloy 617 exhibits classical primary, secondary, and tertiary regimes under some conditions; it often displays a relatively short primary and secondary creep regime followed by a lengthy tertiary creep regime prior to rupture. Thus, the onset of tertiary creep based on the classical definition occurs at very short time.

The three stages of typical creep curves are the result of microstructural changes. Primary creep involves the generation, glide and entanglement of lattice dislocations resulting in hardening. Secondary creep is thought to represent the balance between hardening and recovery mechanisms. The onset of tertiary creep, (i.e., the transition from secondary to tertiary creep) behavior, is poorly understood. In austenitic stainless steels, onset of tertiary creep is associated with extensive cavitation. For other alloys including Alloy 617, Grade 91 steel and Alloy 800H this is not necessarily the case. For these materials although creep void growth and linkup are responsible for failure, cavitation is not the root cause of the transition to tertiary creep. An alternate mechanism dominating the onset of tertiary behavior is required for Alloy 617, as discussed below in detail.

## POROSITY STUDY OF INTERRUPTED CREEP TESTS

### Optical Metallography

The average porosity in the gage section as a function of the interrupted creep strain is plotted in (Figure A-1) At 750°C (Figure A-1a), creep porosity fractions are very small – even at very high total creep strains of 20%. Also, the porosity fraction that develops at a given interrupted strain does not appear to be strongly dependent on the initial creep stress. At 1000°C (Figure A-1b), creep porosity is not evident below approximately 5% creep strain and only becomes significant when the total creep strain exceeds about 10%, with the exception of the creep test run at 1000°C and 10 MPa. Above a total creep strain of 5%, the porosity fraction steadily increases as the creep strain increases. Also, at 1000°C, higher levels of porosity develop at lower values of the initial creep stress for a given total creep strain, Figure A-1b. This is especially evident for an interrupted creep strain of 20% where relatively little creep porosity is found in samples tested at high initial creep stress values of 56 and 70 MPa compared to samples tested at 16 and 20 MPa.
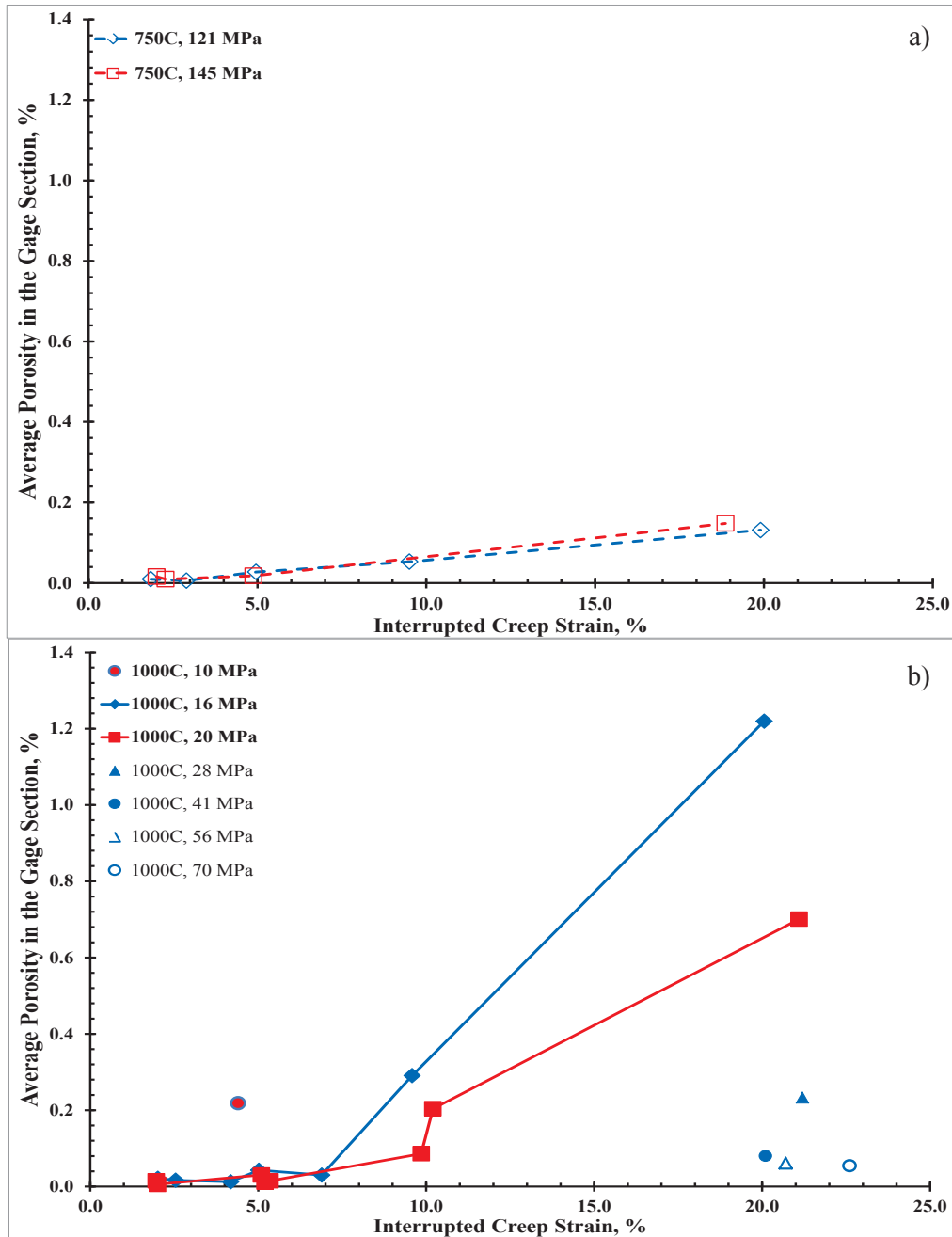
Figure A-1. Plots showing the relationship between creep porosity and the interrupted creep strain for a) 750°C and b) 1000°C.

The average creep porosity as a function of the tertiary creep strain (total creep strain minus the strain attributed to primary and secondary creep), has been plotted in Figure A-2 for tests run at 1000°C. Porosity is negligible at the beginning of the tertiary creep regime and increases with increasing tertiary creep strain and the time spent in the tertiary creep regime. The fractions of porosity at the start of the tertiary regime are too low to significantly affect the stress in the gage section, thus, the accelerated creep rate in this region is likely caused by another mechanism.
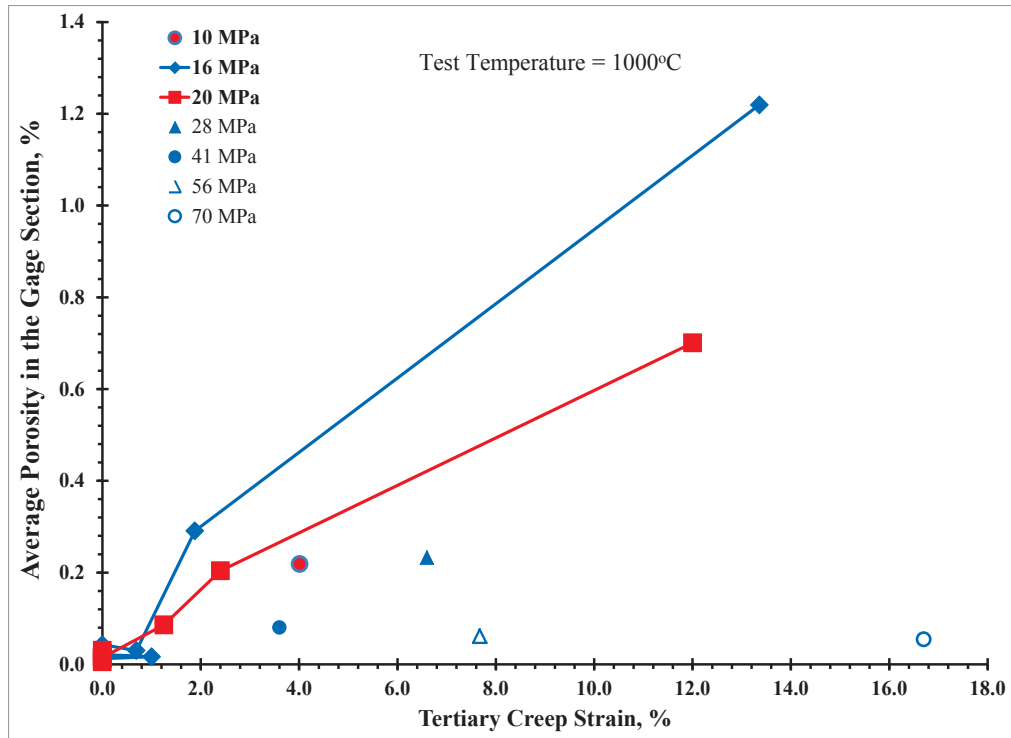
Figure A-2. The influence of the creep strain accumulated during tertiary creep.

# Transmission Electron Microscopy

TEM was used to search for significant amounts of porosity on a scale below the resolution of optical microscopy and/or search for other explanations for the rapidly increasing creep rate in the tertiary regime exhibited by Alloy 617. Possible evidence of creep cavitation on a microscopic level was found in only one area during TEM examinations, even on creep samples subjected to more than ~10% total creep strain (and tertiary creep strain in excess of 2%). Thus, incidences of creep cavitation are deemed to be rare in TEM examinations and insignificant in affecting the creep behavior. The creep cavitation measured in optical micrographs includes virtually all the creep porosity that developed in the samples during creep testing.

## 0.7% Tertiary Creep Strain at 16 MPa and 1000°C

Micrographs in the top row of Figure A-3 indicate the dislocation substructure is more organized than in samples without any tertiary creep strain and the grain interior is relatively free of individual dislocations. Figure A-4c shows a grain boundary precipitate as a source of dislocations, most likely due to strains associated with thermal expansion mismatch between the precipitate and the matrix. No evidence of creep cavitation on a microscopic level was detected in these samples.

## 1.3% Tertiary Creep Strain at 20 MPa and 1000°C

Micrographs in the middle row of Figure A-3 show the microstructure associated with approximately twice the level of tertiary creep strain as that shown in the top row. The dislocation density is elevated with dislocation slip bands evident; the dislocations in the sub-grains are more organized with evidence of dislocation-dislocation reactions that form lower energy boundaries (see arrow).

## 2.4% Tertiary Creep Strain at 20 MPa and 1000°C

    Micrographs in the bottom row of Figure A-3 are representative of almost twice as much tertiary creep strain as those of in the middle row (and almost 4 times that of the top row). Grain interiors are relatively free of lattice dislocations. Dislocation slip bands are not as prevalent but the dislocation cell walls are more developed. No creep cavitation was observed in any of these samples.
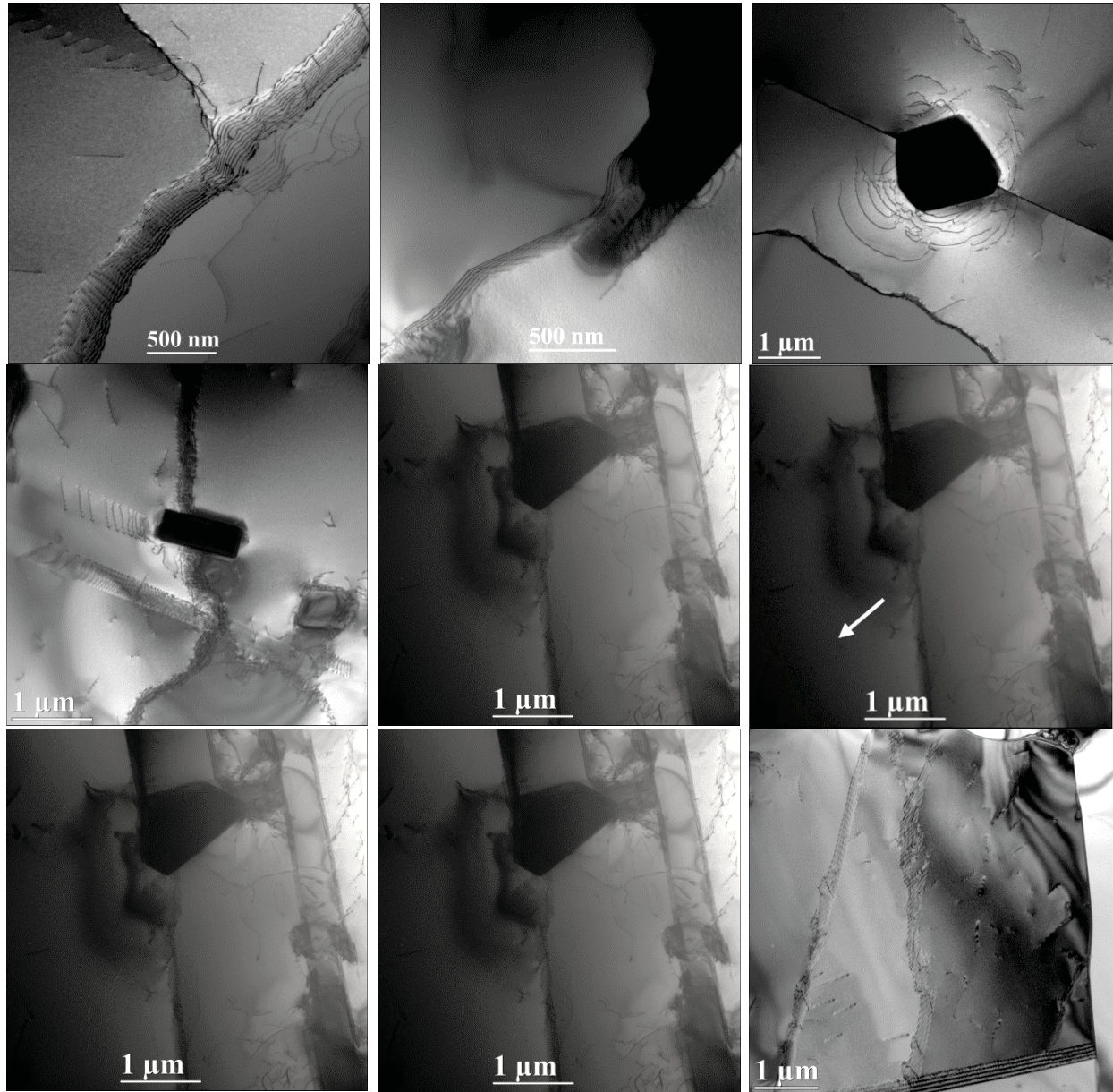


Figure A-3. TEM micrographs from sample taken from the gage section of interrupted creep samples with various amounts of tertiary creep, (top row) 16 MPa, 0.7% tertiary creep strain (~7% total creep strain), (middle row) 20 MPa, ~1.3% tertiary creep strain (~10% total creep strain) and (bottom row) 20 MPa, ~2.4% tertiary creep strain (~10.2% total creep strain).

# Root Cause of the Transition to Tertiary Creep Behavior

The main conclusion that can be drawn from the information presented here is that the transition to tertiary creep is not due to creep cavitation and the associated reduction of the effective cross sectional area of the gage diameter. Significant amounts of creep cavitation on a microscopic level were not found during TEM examinations, even on creep samples subjected to more than ~10% total creep strain (and tertiary creep strain in excess of 2%). Therefore, the creep cavitation measured in optical micrographs includes virtually all the creep porosity that developed in the sample during creep testing. The reduction in the effective cross sectional area due to creep porosity at the transition to tertiary creep behavior is small (<1%) and unlikely to result in the rapidly increasing creep rate exhibited in the tertiary creep regime of this alloy. The transition to tertiary creep is more likely due to another mechanism: softening associated with formation of well-organized dislocation boundaries. Evidence in support of the formation of low energy dislocation substructures was observed and is thought to be responsible for the transition to tertiary behavior by a growing number of researchers [A1-A5]. Figure A-4 show instances of the formation of highly geometric dislocation structures within cell walls. These geometric structures can only be made by rearrangement and interaction of dislocations within the cell wall to form low energy dislocation structures. These low energy dislocation networks effectively reduce the dislocation density, and increase the mean-free path of mobile dislocations during creep, as well as reduce the long range stresses arising from dislocation cell walls that would arise from less organized dislocation networks.
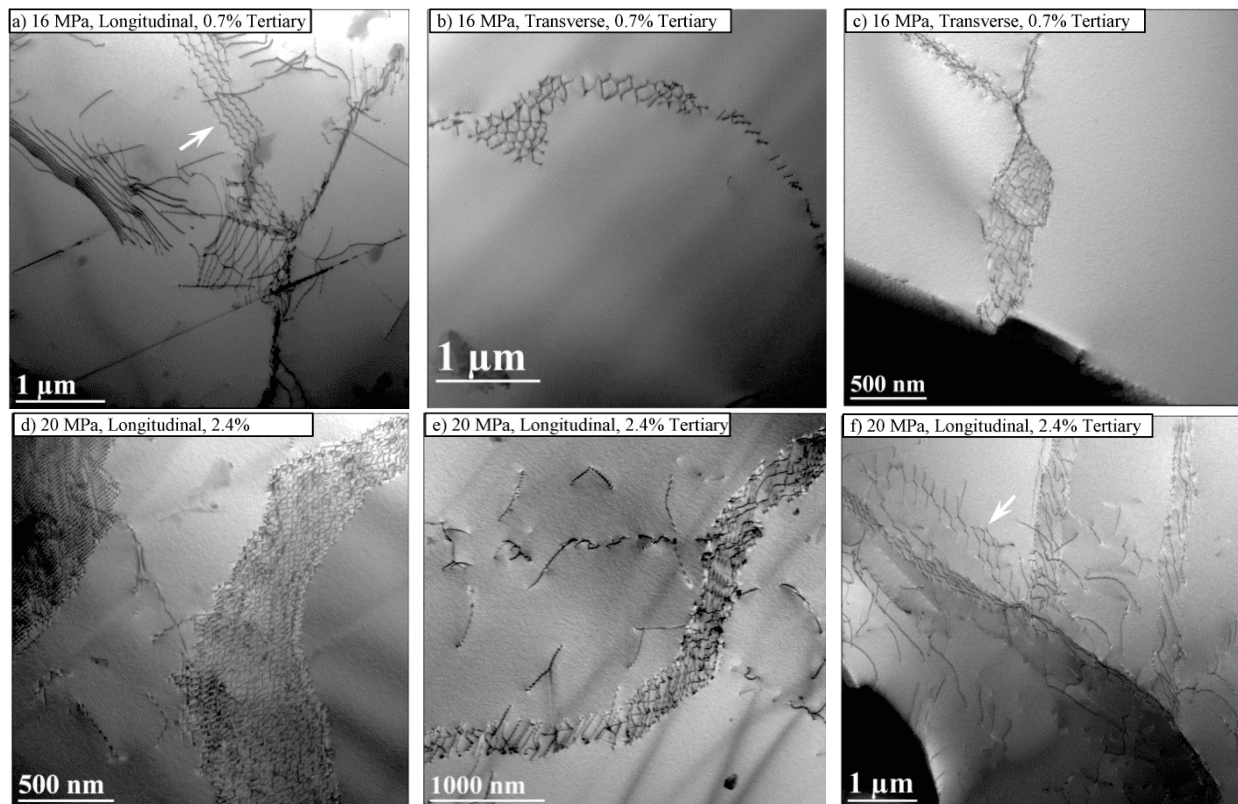


Figure A-4. Examples of the formation of dislocation networks during creep in the tertiary regime.

# REFERENCES

[A1] F. Prinz, A. S. Argon, and W. C. Moffat, "Recovery of dislocation structures in plastically deformed copper and nickel single crystals," Acta Metall., vol. 30, pp. 821–830, 1982.

[A2] A. K. Mukherjee, J. E. Bird, and J. E. Dorn, "Experimental Correlations for High Temperature Creep," Trans. ASM, vol. 62, pp. 155–179, 1969.

[A3] S. Takeuchi and A. S. Argon, "Review: Steady-state creep of single-phase crystalline matter at high temperature," J. Mater. Sci., vol. 11, pp. 1542–1566, 1976.

[A4] M. C. Carroll and L. J. Carroll, "Developing Dislocation Subgrain Structures and Cyclic Softening During High-Temperature Creep-Fatigue of a Nickel Alloy," Metall. Mater. Trans. A, vol. 44A, pp. 3592–3607, 2013.

[A5] J. L. Martin and A. S. Argon, "Low Energy Dislocation Structures due to Recovery and Creep," Mater. Sci. Eng., vol. 81, pp. 337–348, 1986.